GEOMAGNETICALLY INDUCED CURRENT CHARACTERISTICS IN SOUTHERN AFRICA

A thesis submitted in partial fulfilment of the
requirements for the degree of

MASTER OF SCIENCE

of

RHODES UNIVERSITY

by

CHIGOMEZYO MUDALA NGWIRA

June 2008

Abstract

Geomagnetically induced currents (GICs), resulting from adverse space weather, have been demonstrated to cause damage to power transformers at mid-latitudes. There is growing concern over possible GIC effects in the Southern African network due to its long power lines. Previous efforts to model the electric field associated with GICs in the Southern Africa region used a uniform ground conductivity model. In an effort to improve the modelling of GICs, GIC data together with Hermanus Magnetic Observatory geomagnetic field data were used to obtain a multilayered ground conductivity model. This process requires a definition of the network coefficients, which are then used in subsequent calculations. This study shows that GIC computed with the new network coefficients and the multilayered ground conductivity model improves the accuracy of GIC modelling. Then GIC statistics are derived based on the recordings of the geomagnetic field at Hermanus, the new network coefficients and ground conductivity model. The geoelectric field is modelled using the plane wave method.

The properties of the geomagnetic field, their time derivatives and local geomagnetic indices were investigated to determine their characteristics in relation to the GIC. The pattern of the time derivatives of the horizontal geomagnetic field closely follow the rate of change of the north-south geomagnetic component rather than the east-west component. The correlation between the GIC and the local geomagnetic field indices was also investigated. The results show that there is a higher correlation between the GIC and the east-west components of the geomagnetic local indices than between the GIC and the north-south components. This corresponds very well with the orientation of the power lines feeding the power transformers at the South African Grassridge electrical substation GIC site. Thus, the geoelectric field driving the GIC at Grassridge is north-south oriented. Further, it is shown that the geomagnetic observation sites have a strong directional preference with respect to the Grassridge GIC site.

Acknowledgements

First and foremost I would like to thank my supervisors, Dr. Lee-Anne McKinnell and Dr. Pierre Cilliers for their invaluable contributions. The successful completion of this work would not have been possible without their guidance and motivation. The work for this thesis was carried out at the Hermanus Magnetic Observatory. I wish to thank management and staff for their support, in particular Emmanuel Nahayo, Lindsay Magnus and Dr. Ben Opperman. I extend my gratitude to Prof. Trevor Gaunt of the University of Cape Town for providing the GIC data and for his support. This work would not have been possible without the financial support of the National Astrophysics and Space Science Programme of South Africa.

A special word of thanks to Dr. Antti Pulkkinen of the Finnish Meteorological Institute, but currently at NASA/GSFC, who made possible the work on the ground conductivity model. My sincere gratitude for the advice and timely help. On a number of occasions he went out of his way to make this work possible and I cannot thank him enough but to call him a dear friend. Thankyou to Dr. Risto Pirjola and Dr. Larisa Trichtchenko for their support and continued interest in this work. Dr. Pirjola was a great encouragement and introduced me to many people that contributed to this work. In a sense he was the "unofficial" supervisor of this work. Dr. Ari Viljanen cannot go without mention. I extend my thanks to him for all the help and guidance provided. I also thank Mark Hamilton of Dublin Institute for Advanced Studies and Peter Fernberg of the Canadian Geological Survey for their assistance. Dr. Alan Jones of Dublin Institute for Advanced Studies made valuable comments on the validity of the 1-D conductivity models for South Africa.

To work away from home is perhaps one of the more difficult challenges I met during my course of study. I would like to thank my family and friends for their support and faith in me. I thank my late parents Mr. R. D. K. Ngwira and Mrs. J. G. Ngwira for having invested in my education.

Finally, I thank the Lord Almighty for being with me even in times when I had lost all hope. Eight years ago, I did not believe that I could come this far. Surely, the grace of the Lord has seen me through the most difficult times in my life.

Chigomezyo Mudala "Makalanga" Ngwira
Hermanus, South Africa.
June 2008.

Contents

List of Tables

List of Figures

Chapter 1

Introduction

1.1 Geomagnetically induced currents

Geomagnetically induced currents (GICs) occur at the end of the space weather chain which originates from the Sun. Space weather is a term used to refer to the conditions on the sun, in the solar wind, the magnetosphere and the ionosphere that can influence space and ground man-made technologies (Pulkkinen, 2003, and references herein). Major disturbances of the Earth's magnetosphere can occur when the interplanetary magnetic field (IMF) turns southward and remains southward for a long period of time while the Earth is engulfed in an enhanced solar wind. The magnetosphere responds dramatically to changes in the orientation of the IMF because its major source of energy is through its interaction with the solar wind. Increased energy input into the magnetospheric system creates the condition for dynamic changes in the magnetospheric electric current system. Some of this energy goes into driving various magnetospheric processes such as magnetic storms, which are characterised by enhanced convection of the magnetospheric plasma and an enhancement of the magnetospheric-ionospheric current system. Further, part of the energy goes into driving various magnetospheric processes such as the ring current circulating the Earth (Pulkkinen, 2003, and references herein), while some is stored in the magnetotail and released later in substorms.

Geomagnetic field disturbances caused by magnetic storms result in geoelectric potential differences at different points on the Earth's surface which give rise to GICs (Boerner *et al.*, 1983). GICs are a source of concern in man-made techno-

logical systems such as railway lines, oil pipelines, telecommunication cables and power transmission grids. The frequency range of GICs is about 0.01-1 Hz. For an AC power transformer operating at a frequency of 50 or 60 Hz, this is seen as a quasi-DC current. GICs flowing through the windings of power transformers produce extra magnetic flux that causes half cycle saturation leading to transformer heating and increased power demand. These effects tend to shorten the operational life time of transformers and causes failure of protective devices such as relays and circuit breakers (Boteler, 2001; Boerner *et al.*, 1983). Transformer core saturation creates power line harmonic radiation which increases during periods of increased geomagnetic activity and in extreme cases the combination of these effects can have a serious impact on the transmission system stability and lead to power blackouts.

Perhaps the best known example of the devastating effects of GICs on power systems is that which occurred during the 13 March, 1989 superstorm (Boteler, 2001, and references herein). The GIC events following the superstorm caused a blackout on the entire Hydro-Quebec power system in Canada on a time scale of just one-and-a-half minutes. The power outage was the result of wide spread transformer saturation and affected about 6 million people. It also cause extensive damage to the infrastructure of the system. During the same event, a generator step-up power transformer was destroyed in New Jersey, USA. The cost of replacing such equipment is very high, but the financial losses to power companies as a result of such blackouts are even higher.

Society today relies heavily on electricity in order to meet essential needs. To meet the rising demand for this energy, power companies require smooth and efficient delivery of services to the consumers. By extending the grid, Southern African power companies are trying to ensure that the needs of our society are met. However, the network expansion programme increases vulnerability to the potential effects of GIC which build up cumulatively over large geographic scales because of very long conductors, and may overwhelm protection margins of equipment and the capacity of the system to regulate voltage. This is evident from the transformer failures experienced in November 2003 at some substations following a series of geomagnetic events in October and November of the same year as reported by Gaunt

and Coetzee (2007).

The flow of GICs in a power system is strongly influenced by the configuration of the power system, the system parameters (such as network resistances and coefficients) and the ground conductivity. There are a number of ways to prevent the flow or limit the effects of GICs on power transformers. These include the use of 3-phase 3-legged core type transformers which are less susceptible to saturation by GIC or placing blocking capacitors in the power transmission lines (Boteler, 2001). However, these solutions are not considered economical by the power companies and thus more economical approaches must be sought.

Many studies have been undertaken in Finland, Canada, USA, UK, and other areas faced with these problems in order to find more economical means of preventing or mitigating the space weather effects (Kappenman *et al.*, 1997; Boteler, 2001; Pirjola, 2002c; Thomson *et al.*, 2005, e.g.). However, these studies were done at higher latitudes where the effects are most common and severe due to auroral activity in these regions near the magnetic poles. There is very little published data on GICs in the Southern African region, because it was assumed that GICs could not exist at low to mid latitudes (Gaunt and Coetzee, 2007). Therefore, a lot of effort is being spent to learn what has been done in other regions in order to understand the mechanisms associated with GICs and to use this knowledge to characterise GICs in our region. The desired goal is to develop models that are applicable to our region.

1.2 Overview of GIC studies in the region

Koen (2002) established the existence of GICs in the Southern African network. Because it is a mid-latitude region, it was thought that GICs do not exist or pose any real threat (Gaunt and Coetzee, 2007). Koen (2002) applied the plane wave model with an assumed uniform layer ground conductivity model to calculate the GIC at particular stations. In his thesis, he investigated the occurrence of GICs in the Southern African power network by considering geomagnetic data only from Hermanus Magnetic Observatory (HMO, $19.2\,^{\circ}E$, $34.4\,^{\circ}S$) and GIC data from the different GIC monitoring sites across South Africa. His assumption was that the

geoelectric field pattern across the whole region covered by the network was uniform and thus he could use the magnetic field at HMO to model GICs at a site over 500 km away.

Zatjirua (2005), using methods similar to Koen's, investigated the existence of GICs in the transmission network of Namibia, using geomagnetic field measurements recorded at the geomagnetic station at Tsumeb (TSU, $17.4\,^{\circ}E, 19.2\,^{\circ}S$). No GIC monitoring sites were in existence then and to date there are still none on this network, but what is clear from this investigation is that transformer failures were noted that agree very well with geomagnetic events that caused similar problems in the South African system. According to Zatjirua's model, GIC currents as much as 17 A and above could exist on the Namibia network during severe storm events such as the Halloween storm of 29-31 October, 2003.

A later study by Bernhardi (2006) investigated and implemented the method of Spherical Elementary Current Systems (SECS) to interpolate the magnetic field between measurement locations. The SECS method involves the derivation of equivalent ionospheric currents and allows one to get accurate ground magnetic field measurements at a site of interest. The SECS method was developed by Amm (1997) and Amm and Viljanen (1999) and was comprehensively used by Pulkkinen (2003). Bernhardi's study showed that the electric field is not spatially uniform. The spatial variation of the field during a geomagnetic event is illustrated in Figure 1.1. Bernhardi (2006) concluded that there is a need to consider data from other observatories around the region, especially the ones closest to the point of interest.

The geoelectric field at the Earth's surface driving the GIC is very sensitive to the sub-surface electrical conductivity structure. It is therefore important that magnetic fields at a monitoring site are accurately determined because the voltages induced in the conductors closest to the site account for the largest contribution to the GICs (Viljanen *et al.*, 2004). Viljanen *et al.* (2004) report that earlier attempts to calculate the induced currents failed due to the use of magnetic data from distant locations. One must take into account that the geoelectric field is not spatially uniform in the higher latitude auroral regions.

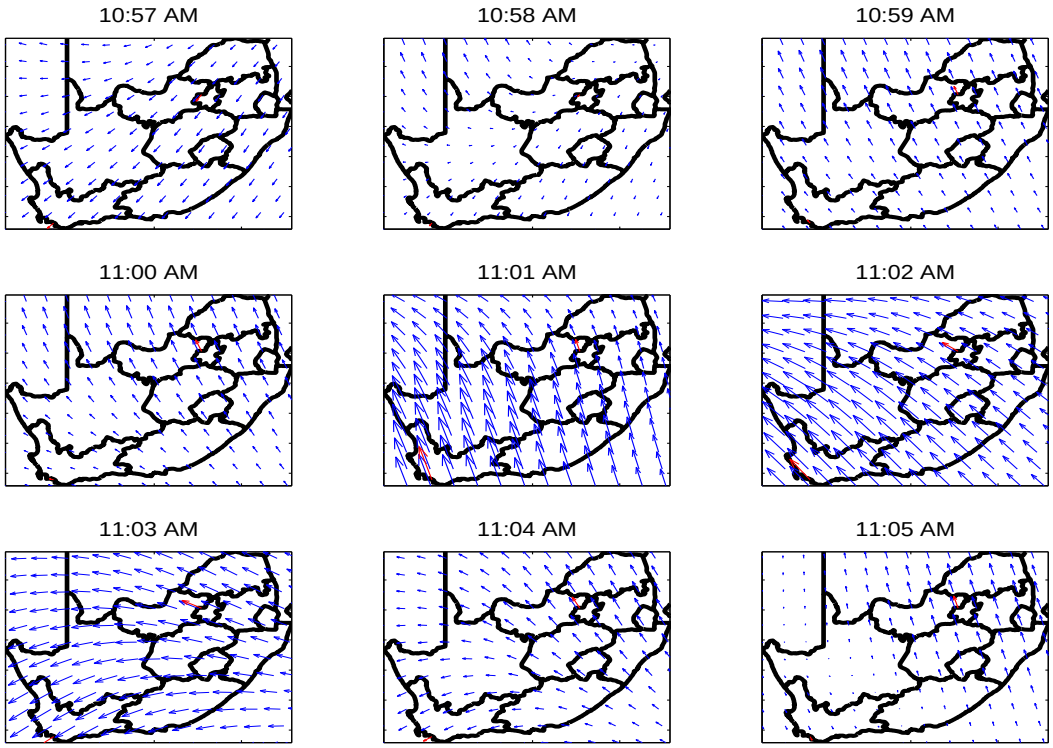

Figure 1.1: Variation of the electric field across South Africa as investigated by Bernhardi (2006).

1.3 The purpose of this study

GICs have been identified in the Southern African power grid (Koen, 2002) and hence there exists a strong necessity to study and characterise parameters that are closely related to the GIC in order to improve the modelling efficiency of GICs in the Southern Africa power transmission network. The development of such a model would greatly assist power companies in power grid management and mitigation of the impact of space weather on their systems and thus enhance the delivery of uninterrupted power services to the consumers. The motivation for this work has been the growing concern over the possible effects of large geomagnetic storms which frequently occur during the descending phase of the solar cycle. The aims of this study fall into two categories:

- The improvement of the ground conductivity model and the subsequent modelling of GICs in Southern Africa.
- The determination of parameters that can be used to characterise the GIC

events on the power network.

The two categories are outlined below:

Model calculation of GICs in a network depends on the fairly accurate determination of the geoelectric field and the network coefficients. Network coefficients are characteristics particular to each power transformer and power line which depend on the power system geometry and resistances (Viljanen and Pirjola, 1989, 1994). The geoelectric field is strongly influenced by the ground conductivity. Previous efforts to model the electric field used the plane wave model with a uniform one-layer ground conductivity (e.g. Koen, 2002; Zatjirua, 2005). In the first part of this study a ground conductivity model that would improve the accuracy of GIC modelling by the inclusion of a more realistic layered ground conductivity structure, was developed. This is important for the future development of a reliable and optimal GIC monitoring system.

There is very little published data on the geophysical aspect of the GICs in the mid and low latitude regions. In order to understand the scope of GICs, it is important to characterise the related parameters. Thus, the second part of this thesis reports on a study to understand and characterise GIC events in the region. The ultimate goal is to determine which parameters can be used as indicators of the severity of the geomagnetic storm for the purpose of classification of the local storm conditions in relation to the expected GIC levels on the network.

1.4 Data sources and limitations

Geomagnetic field 1-minute mean data values available at the HMO (for the three observatories in Southern Africa managed by the HMO) were used in this study for all ground-based magnetic measurements. Data from Hartebeesthoek (HBK, $27.7\,^{\circ}E, 25.9\,^{\circ}S$) and Tsumeb observatories were used whenever data was available to make comparisons on a larger regional scale than just in the near vicinity of the HMO. The X, Y and Z components were recorded using a three-axis suspended FGE fluxgate magnetometer manufactured by the Danish Meteorological Institute.

Monitoring of GICs in the South African power grid commenced in 1998 under the EPRI Sunburst project. GICs had previously only been recorded at two Eskom power transformer sites i.e. Grassridge ($25.6\,^{\circ}E, 33.7\,^{\circ}S$) and Hydra ($24.09\,^{\circ}E, 30.71\,^{\circ}S$). To aid our comparisons, 2-second GIC data recorded at the Sunburst site was averaged to a 1-minute sampling interval.

It is important to stress that GIC studies in Southern Africa are limited due to a lack of measured GIC data. Availability of data is very important when developing a model. The only available GIC data was for the three-day storm period of 29-31 October, 2003 at Grassridge. This data is not enough. One needs data that covers at least one solar cycle, because geomagnetic events vary with the cycle. Thus more data is needed to carry out a comprehensive analysis of the relationship between the GIC and geomagnetic parameters.

Aggravating the situation is the very small number of existing magnetic observatories covering this vast region. The lack of relevant data makes it difficult to model and determine the true extent of GIC existence and the possible risk it poses to the network. Most of the observatories in Southern Africa considered in this study are very far from the GIC recording sites. In this thesis we make use of the available resources and all conclusions drawn are based on the results obtained.

1.5 Structure of the thesis

Chapter 2 reviews the theoretical foundations on which the work presented in this thesis is based. The chapter begins by looking at the origins of the space weather and the propagation of the solar wind through interplanetary space to its subsequent interaction with the Earth's magnetosphere. The processes in the magnetosphere and ionosphere resulting from the interaction with the solar wind are then described. The chapter ends by looking at the ground level effects of these processes and the methods available to derive quantities of interest and finally the actual modelling of the GIC which is at the end of the space weather chain.

Chapter 3 looks at the derived layered ground conductivity model and its subsequent validation. A new set of network coefficients which were used in the deriva-

tion of the layered ground model are introduced. The derived layered ground conductivity model is presented and then it is established that this model improves the accuracy of GIC modelling. It is then demonstrated that the derived layered ground conductivity model degrades with increasing distance from the geomagnetic observation site and that it is valid only for the specific geomagnetic observatory and GIC station pair. Based on the new ground model and network coefficients, a statistical analysis of the frequency of occurrence of GICs in the network is conducted.

The characteristics of the geomagnetic field and its time derivatives are investigated in Chapter 4. An analysis of the correlation between the model GIC and the geomagnetic range indices and also between the model GIC and the hourly standard deviation is presented. The dependence of geomagnetic activity upon diurnal, seasonal and solar cycle variations are investigated based on the hourly standard deviation. The chapter concludes by looking at the improvement in correlation coefficients when measured GIC data is used in the analysis.

The findings of this work are summarised and the conclusions are drawn in Chapter 5.

Chapter 2

Theoretical background

In this chapter, basic theoretical principles associated with GIC studies are reviewed. The review begins by looking at the solar origins of space weather, then at the solar wind propagation through interplanetary space and its subsequent coupling with the magnetosphere and down to the induction effects on the power grids. This review emphasises the ground level events.

2.1 The Sun

The Sun is a medium-sized star and the Earth's primary source of energy. Without this energy, life on Earth would not be sustainable. However, the Sun is also a source of space weather which seriously affects man-made technologies both in outer space and on Earth. The Sun has a magnetic field which varies with the 11-year solar activity cycle. The magnetic field is associated with a number of observable phenomena that take place on the surface of the Sun such as sunspots, solar flares, coronal mass ejections, prominences and filaments. Part of this magnetic field travels into interplanetary space moving together with the solar wind as a plasma of electrons and ions. A number of books have been published bearing detailed discussions of the processes occurring on the Sun which are not looked at here (e.g. Kivelson and Russell, 1995; Walker, 2005, and references therein).

2.1.1 Sunspot cycle

Sunspots are regions on the Sun's surface with lower temperatures than their surroundings and thus appear as dark spots relative to their surroundings. Individual spots may have a lifetime that ranges from about an hour to several months. Sunspots have a tendancy to occur in pairs, have intense magnetic fields and are a source of solar flares and coronal mass ejections (Campbell, 1997, Chapter 3). The number of sunspots visible on the solar surface varies with the 11-year solar cycle which is marked by increased (solar maximum) or decreased (solar minimum) geomagnetic activity. Intense solar storms are experienced 2-3 years after the peak of the sunspot cycle (Campbell, 1997; Beamish *et al.*, 2002). Figure 2.1 shows the sunspot cycle from the year 1900 to 2007.

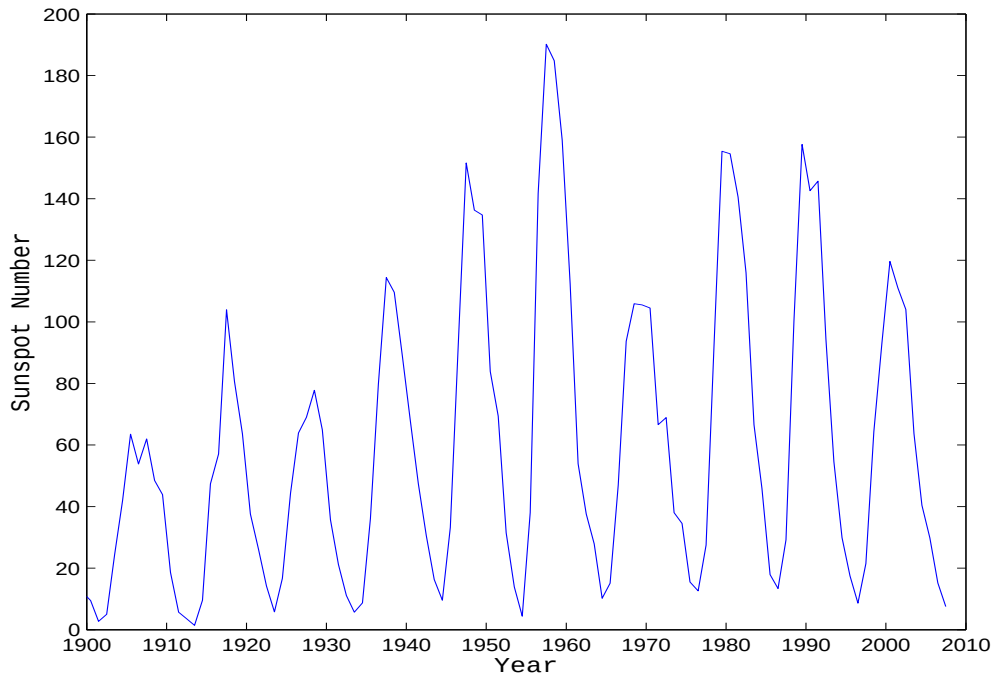

Figure 2.1: Sunspot cycle from the year 1900 to 2007.

2.1.2 Coronal mass ejections

Coronal mass ejections (CMEs) are ejections of huge amounts of plasma from the surface of the Sun into interplanetary space. The plasma carries with it part

of the Sun's magnetic field in the form of the solar wind. After a CME event, the solar wind travels at high speeds and has a colossal amount of energy. The occurrence of CMEs is associated with closed magnetic field lines and can take place at any time during the solar cycle (Campbell, 1997, Chapter 3). The rate of CME occurrence increases with increasing solar activity which tends to peak during solar maximum (Campbell, 1997; Richardson *et al.*, 2001). Richardson *et al.* (2001) and Huttunen *et al.* (2002), report that CMEs are the major cause of most geomagnetic storms around solar maximum and Richardson *et al.* (2001) further state that the majority of the *intense* geomagnetic storms observed at solar maximum are essentially CME-related.

2.1.3 Solar wind and interplanetary magnetic field

The solar wind is the outflow of plasma from the Sun's surface into interplanetary space. It is not uniform (variable magnitude and direction) but is always directed outward from the Sun. The solar wind carries with it magnetic clouds, which are interacting regions where the high speed wind catches up with the slow speed wind (Zhang *et al.*, 2004). Solar wind speed can be about 300 $\mathrm{km\,s^{-1}}$ during quiet times and more than 650 $\mathrm{km\,s^{-1}}$ during storm times. Richardson *et al.* (2001) have shown that a slow solar wind speed is responsible for the generation of a small number of weaker storms during solar minimum and maximum. High speed solar winds interacting with the Earth's magnetic field can produce large storms in the Earth's magnetosphere depending on the composition of the solar wind parameters. *In-situ* space satellites provide information about the conditions of the solar wind (i.e. velocity, temperature, density and the magnetic field components etc.).

The Interplanetary Magnetic Field (IMF) is a part of the Sun's magnetic field that is carried by the solar wind. Due to the rotation of the Sun and the frozen-in-flux condition, the IMF travels outward in a spiral pattern originating from regions on the Sun where open magnetic field lines emerging from one region do not return to a conjugate region but instead extend indefinitely into space. The frozen-in-flux condition implies that if at a given time t_0, an element of particles exists on a particular field line, then at a later time t_1, this element of particles will still be on the same field line (Campbell, 1997; Walker, 2005). The interaction of the IMF with the Earth's magnetic field is responsible for the shape of the magnetosphere

and is one of the important conditions that determines the processes that yield geomagnetic storms.

The IMF is described by three orthogonal component directions B_x, B_y, and B_z. The directions of the IMF are important for the study of the interaction of the solar wind with the magnetosphere. Campbell (1997) reports that the accepted model for the IMF supposes that when the southward directed IMF ($-B_z$ IMF) encounters the northward directed magnetic field of the Earth, then the field lines interconnect, distorting the Earth's dipole field and providing entry for the solar wind particles into the magnetosphere through the process of magnetic reconnection. The southward turning IMF ($-B_z$) becomes the requirement for the initiation of major magnetic disturbances on the Earth (Campbell, 1997; Richardson *et al.*, 2001; Rosenqvist *et al.*, 2005; Walker, 2005). During reconnection, there is an increased energy input into the magnetospheric system which initialises the conditions for dynamic changes within the magnetospheric current systems.

2.2 The Magnetosphere

The magnetosphere can be viewed as the cavity housing the Earth's magnetic field. The dynamics of the plasma and energetic particles within the magnetospheric cavity are strongly influenced by the Earth's magnetic field. The magnetosphere extends upward for several Earth radii with the ionosphere as its lower boundary (Matsushita and Campbell, 1967; Walker, 2005). The formation and extent of the outer region of the magnetosphere are mostly determined by its interaction with the interplanetary medium (including the solar wind). Solar activity is known to strongly influence the shape and size of the magnetospheric cavity on both the day side (Sunward) and night side (away from Sun).

During a solar storm, the high speed particles ejected from the Sun exert pressure on the magnetosphere compressing it on the day side and extending it far out on the night side forming a tadpole-like feature. At such times, phenomena such as geomagnetic storms and auroras are experienced depending on the intensity of the solar storm. At about 4 Earth radii away from the Earth's surface, particles are fully ionised and are subject to the effects of the electric and magnetic fields.

The density of these particles is very low, thus they tend to behave independently rather than as part of the plasma. The particles exhibit three kinds of motions; gyration about the main field, bounce along the field lines or drift in rings around the Earth. The ring current is one of the major current systems in the Earth's magnetosphere which influences the surface magnetic field. The dynamics of the magnetosphere are better understood today with the help of satellites and scatter radar measurements.

2.2.1 Ionospheric currents

Ionospheric currents responsible for the magnetic disturbances that affect power systems at mid to high latitudes are associated with two different processes in the magnetosphere, magnetospheric convection and magnetic reconnection. During storm events, current systems in the ionosphere and magnetopause are modified and on the ground these are observed as deviations of the local geomagnetic fields (Nishida, 1978; Kivelson and Russell, 1995). In the polar caps and the auroral zones, the eastward and westward convection electrojets form part of a two cell current circulation resulting from the convection of magnetic field lines inside the magnetosphere as a result of energy coupling from the solar wind. The loading of energy into the magnetotail and its subsequent unloading into the auroral ionosphere leads to substorms which can cause rapid magnetic field variations producing power system problems.

2.3 Geomagnetic field

The surface magnetic field of the Earth is measured at different magnetic observatories distributed around the world. The field is represented by three orthogonal vector components **X** (north), **Y** (east) and **Z** (vertical) with respect to the geographical coordinate system. It is important to note that the **Z** component points upward in the southern hemisphere. The **X** and **Y** together are used to obtain the horizontal intensity (**H**) given by $H = \sqrt{X^2 + Y^2}$. The increase in the **H** field component is usually detected at the beginning of magnetic storms at low to mid latitude observatories. The measure of the deviation of the geomagnetic **H** field from the geographical North is the declination D and the dip of the total

field with respect to the horizontal plane is measured by the inclination angle I (Kivelson and Russell, 1995; Campbell, 1997). Geomagnetic activity varies during storm times and the variations depend on the geoeffectiveness of the interplanetary parameters. Geoeffectiveness is used here in reference to the ability of a given storm to give rise to considerable GIC levels. High levels of geomagnetic activity affect communication operations, cause oil pipeline corrosion and are the primary drivers of GICs in power transmission lines.

The study of GICs is usually divided in two independent parts (Pirjola, 2000). The first (geophysical) is the determination of the geoelectric field based on the knowledge of ionospheric equivalent currents and ground conductivity models, while the second (engineering) is the computation of the GICs driven by the determined electric field. The former is based on a knowledge of the power network details (or system parameters). This section looks at the processes involved in the geophysical aspect and section 2.4 briefly looks at the engineering aspect.

2.3.1 Geomagnetic storms

The Sun is the major driver of magnetic field instabilities on the Earth. The movement of particles trapped in the Earth's inner magnetic field and drifting as mentioned in section 2.2 constitutes the Van Allan radiation belt. The current produced by this drift causes a magnetic field on the Earth's surface similar to that of the large ring of current in the planet's magnetic equatorial plane. The current system causes instabilities in the surface magnetic field at the Earth which in turn gives rise to geomagnetic storms. The word geomagnetic storm refers to a disturbance of the Earth's surface magnetic field. Geomagnetic storms are observed on the Earth only after events such as CMEs, coronal holes, or solar flares, occurring on the Sun, travel in a direction towards the Earth. A solar wind shock arising from such events leads to a modification of the ionospheric current system due to changes in the north-south IMF $-B_z$ component and pressure of the solar wind (Campbell, 1997, Chapter 3).

A typical geomagnetic storm is characterised by three phases: the initial phase (though some storms may occur without the initial phase), main phase and recovery phase. The initial phase is at times marked by a sudden storm commencement

(SSC). The difference in speed between the fast and slow moving solar wind after CME events results in the formation of the solar wind shock, which is responsible for the observed sudden increase in the H component as the shock wave arrives at the magnetosphere boundary prior to the commencement of a geomagnetic storm (Campbell, 1997, Chapter 3). During geomagnetic storms, ring current particle fluxes are increased with a maximum enhancement occurring in the inner ring current. The storm time growth of the ring current can last from 3 to 12 hours and is manifested by the decrease of the Dst index. The Dst is a magnetic index that serves as the standard measure of the ring current activity (Jordanova *et al.*, 2001). This constitutes the main phase of the magnetic storm. In the recovery phase the ring current begins to decay returning to its undisturbed state in 2 to 3 days or more.

2.3.2 Geomagnetic indices

The degree of disturbance of the geomagnetic field serves as a proxy that characterises the level of disturbance in the magnetosphere and ionosphere. Characterisation or indexing is based on a collection of geomagnetic data records. The advantage of indexing is that it helps to sort the geophysical data into activity categories. This process further helps one to establish well-defined parameters that enhance the understanding and interpretation of data. Geomagnetic indexing is based on a selected timescale of variation which is governed by the physical quantity driving the variations (Joselyn, 1995; Kivelson and Russell, 1995).

There are many geomagnetic indices in use today, ranging from local to global scales. Global indices are derived using data of local indices collected from selected magnetic observatory networks. The range of indices in use include the K, Dst, kp, AE, AU, AL, EE, just to mention a few. Some indices such as EE, AE, AU, AL are specific to certain regions as they are used to characterise activities which only affect these particular regions. In this thesis, the local K-index for Hermanus ($19.2\,^{\circ}E$, $33.4\,^{\circ}S$), South Africa has been extensively used in the data selection process.

The K-index is a quasi-logarithmic index of the 3-hourly range in local magnetic activity relative to an assumed solar quiet day curve for each particular geomag-

netic observing site. Its derivation is based on the amplitude of variations in the observed horizontal component. The index is classified into ten disturbance levels with a scale running from 0 to 9 so that 0 is for quiet conditions and 9 for most disturbed conditions (Menvielle *et al.*, 1995; Campbell, 1997; Richardson *et al.*, 2001). The planetary kp index is derived from the local K-index data of 13 magnetic observatories around the world. The K-index has been recorded at Hermanus for more than seventy-five years.

2.3.3 The geoelectric field model

According to Faraday's law of electromagnetic induction

$$\nabla \times \mathbf{E} = -\frac{d\,\mathbf{B}}{dt} \tag{2.1}$$

variations in the horizontal magnetic field induce an electric field which then drives an electric current inside the Earth according to Ohm's law $\mathbf{J} = \sigma\,\mathbf{E}$. The induced electric field observed at the Earth's surface depends primarily on the magnetospheric-ionospheric currents, which in turn are dependent on space weather conditions, while the secondary effects are determined by the conductivity structure of the Earth (Pirjola, 2000). Pirjola (2002b) explains that the horizontal geoelectric field at the surface of the Earth is an important quantity that must be known in order to determine the magnitude of the GIC in the network.

Several methods for calculating the geoelectric field have been established (e.g. Viljanen and Pirjola, 1989; Pirjola and Boteler, 2002; Pirjola, 2002c; McKay, 2003, and references therein). Here, an outline of the principles underlying the plane wave model are reviewed. This model has been chosen merely because it is the simplest model that is in use for GIC studies and is the only method that has been applied to all our regional studies so far.

The geoelectric field at the Earth's surface can be modelled using the plane wave model (Viljanen and Pirjola, 1989; Pirjola, 2002c). Taking the Earth as a uniform half-sphere of conductivity σ and assuming that there is a plane wave field that propagates vertically downwards, then a single frequency ω can be considered, such that the horizontal geoelectric field component E_y can be computed in terms

of the perpendicular horizontal geomagnetic field component B_x (Pirjola, 2002c) as

$$E_y = -\sqrt{\frac{\omega}{\mu_0\,\sigma}}\,e^{\frac{i\,\pi}{4}}\,B_x \tag{2.2}$$

where μ_0 is the permeability of free space and the layer of air between the ground and the ionosphere is considered to have zero conductivity so that there is no significant attenuation of external electromagnetic fields (Simpson and Bahr, 2005, Chapter 2). This equation shows that the magnitude of the geoelectric field increases with increasing frequency and an inverse Earth conductivity.

Eqn. (2.2) can be transformed from the frequency (ω) domain to a time (t) domain by carrying out an inverse-Fourier Transform (Pirjola, 2002c) to obtain

$$E\,(t) = -\frac{1}{\sqrt{\pi\,\mu_0\,\sigma}}\int_0^{\infty}\frac{g\,(t-u)}{\sqrt{u}}\,du = -\frac{1}{\sqrt{\pi\,\mu_0\,\sigma}}\int_{-\infty}^{t}\frac{g\,(u)}{\sqrt{t\,-\,u}}\,du \tag{2.3}$$

where $g\,(t) = d\,\mathbf{B}\,(t)\,/\,dt$. Note that the geoelectric field only depends on the preceding values of the geomagnetic field at any given time. Although this is true, it should also be noted that the most recent values are the most important ones due to the weighting factor $1/\sqrt{t}$ in the integral as the time derivative is a good proxy for the electric field (Pirjola, 2002c).

So then, the plane wave eqn. (2.3) establishes an easier way for estimating the geoelectric field using a time series of the geomagnetic field. If it is further assumed that there is a linearly varying geomagnetic field between successive time steps, then the geomagnetic field according to Viljanen and Pirjola (1989) can be written as

$$B\,(t) = B_{n-1} + \frac{t - T_{n-1}}{\triangle}\,(B_n - B_{n-1}), \quad T_{n-1} \leqslant t \leqslant T_n \tag{2.4}$$

where $\triangle = T_n - T_{n-1}$ is the sampling interval. The geoelectric field at a point $t = T_N$ is then given by

$$E\,(T_N) = \frac{2}{\sqrt{\pi\,\mu_0\,\sigma\,\triangle}}\,(R_{N-1} - R_N - \sqrt{M}\,b_{N-M}) \tag{2.5}$$

M is the number of previous time steps taken into account with $b_n = B\left(T_{n-1}\right)$ and

$$R_N = \sum_{n=N-M+1}^{N} b_n \sqrt{N-n+1} \tag{2.6}$$

The remaining task is to then derive the ground conductivity model to be able to use eqn. (2.5).

2.3.4 Derivation of the ground conductivity

The ground conductivity is a very important parameter used mostly in magnetotelluric (MT) surveys. MT is a method used in the study of the Earth's structure based on the measurement of natural electromagnetic (EM) field (electric and magnetic) fluctuations at the Earth's surface (Simpson and Bahr, 2005, Chapter 1). The difference between the transmitted and received EM fields from MT sounding is evidence of a conducting structure in the Earth and provides information about its geometry and electrical properties (the degree to which the Earth can conduct current). The measurements from MT surveys are represented as a complex impedance tensor which relates the horizontal components of the geoelectric field to the geomagnetic field (Pellerin *et al.*, 1996). The use of the impedance is a very important simplification, because then one can disregard the source-moments and geometry of the source (Hjärten, 2007). The impedance is independent of the amplitude of the electric and magnetic fields.

Over the years, the ground conductivity has found use in the computation of geoelectric fields for GIC studies. The first step in the derivation of a ground conductivity model is to determine the frequency-dependent surface impedance which requires the use of MT methods. The surface impedance provides information about the ground conductivity. The relationship between the horizontal components of the geoelectric field $E_{x,y}$ and geomagnetic field $B_{x,y}$ is given in terms of the surface impedance by

$$E_{x,y}(\omega) = \pm \frac{Z}{\mu_0} B_{y,x}(\omega) \tag{2.7}$$

where $Z = Z(\omega)$ is the surface impedance and ω is the angular frequency. To

reduce the complications in modelling, it is usually assumed that the Earth's conductivity (σ) varies only in the vertical (z) direction i.e. $\sigma(z)$ (Pirjola, 2002c).

The simplest 1-D model assumes that the Earth is a homogeneous half-sphere with uniform conductivity. In GIC studies, the geoelectric field is also a model parameter and would not be ideal for the derivation of surface impedance. However, measured GIC and geomagnetic field data can be used to derive a ground conductivity model as shown by Pulkkinen *et al.* (2007). Using the spectral form of the GIC equation $GIC(t) = a\,E_x(t) + b\,E_y(t)$ (details are given in Section 2.4) and combining with eqn. (2.7) then leads to

$$GIC(\omega) = \frac{Z(\omega)}{\mu_0}\left[a\,B_y(\omega) - b\,B_x(\omega)\right] \tag{2.8}$$

as given by Pulkkinen *et al.* (2007).

Most data contains some unusual observations (or outliers) that do not fit the model distribution. Estimation of Z is thus done using the statistical Robust M-estimator algorithm (Chave and Thomson, 2004; Pulkkinen *et al.*, 2007, and references therein). The ordinary Least Squares (LS) method given by Chave and Thomson (2004) would then yield a solution of the form

$$Z = (\mu_0\,GIC\,B^H)\,(B\,B^H)^{-1} \tag{2.9}$$

where $B = a\,B_y(\omega) - b\,B_x(\omega)$. But the ordinary LS method breaks down and cannot be used due to its sensitivity to the presence of outliers.

However, Robust estimators which are a form of weighted least squares method are insensitive to the presence of a moderate amount of bad data or inadequacies in a model and they react gradually rather than abruptly to perturbations. M-estimators are maximum likelihood estimators for computing robust averages and solving robust regression problems (Chave and Thomson, 2004). The solution is obtained by first carrying out the ordinary LS and then finding the residuals and scaling factors. The residual and scaling factor values are used in the iterative weighted LS given by

$$Z = (B^H \, v \, B)^{-1} \, (B^H \, v \, \mu_0 \, GIC) \tag{2.10}$$

where v is the Huber weighting. This method is effective in eliminating outliers without seriously reducing the statistical efficiency (Chave and Thomson, 2004).

Having determined the surface impedance then allows one to use the standard MT methods to derive the conductivity (Chave and Thomson, 2004; Pulkkinen *et al.*, 2007). The surface impedance is commonly represented in terms of the apparent resistivity $\rho_{a,i}$ (for a nonuniform or layered conductivity) and phase ϕ as

$$\rho_{a,i} = \frac{|\, Z_i \,|^2}{\omega \, \mu_0} \qquad\qquad \phi_i = tan^{-1}(\frac{Im\,[Z_i]}{Re\,[Z_i]}) \tag{2.11}$$

The representation of the Earth's conductivity using a 1-D model allows us to understand the nature of ρ_a and ϕ and the period dependence of the geomagnetic induction (McKay, 2003).

The depth of each layer in the Earth can be determined based on the penetration of the signal which varies with frequency due to the diffusive nature of the electromagnetic fields (Pellerin *et al.*, 1996). It is well-known from MT studies that electromagnetic fields of different periods induce electrical currents at different depths within the Earth due to the effect of "skin depth" (Simpson and Bahr, 2005; Hjärten, 2007). The longer the period of a magnetic signal, the deeper it penetrates the ground as depicted in Figure 2.2.

The resistivity and the conductivity have an inverse relation given by

$$\sigma_i = \frac{1}{\rho_{a,i}} \tag{2.12}$$

The derived conductivity model can then be used in eqn. (2.5) to determine the geoelectric field. It can be shown from the theory of electromagnetic induction that a decrease in the Earth's conductivity leads to an increase in the horizontal geoelectric field. This however, does not mean that networks located in regions which have a high resistivity structure are at a higher risk to GICs since a decrease in the Earth's conductivity tends to increase the earthing resistance which in turn

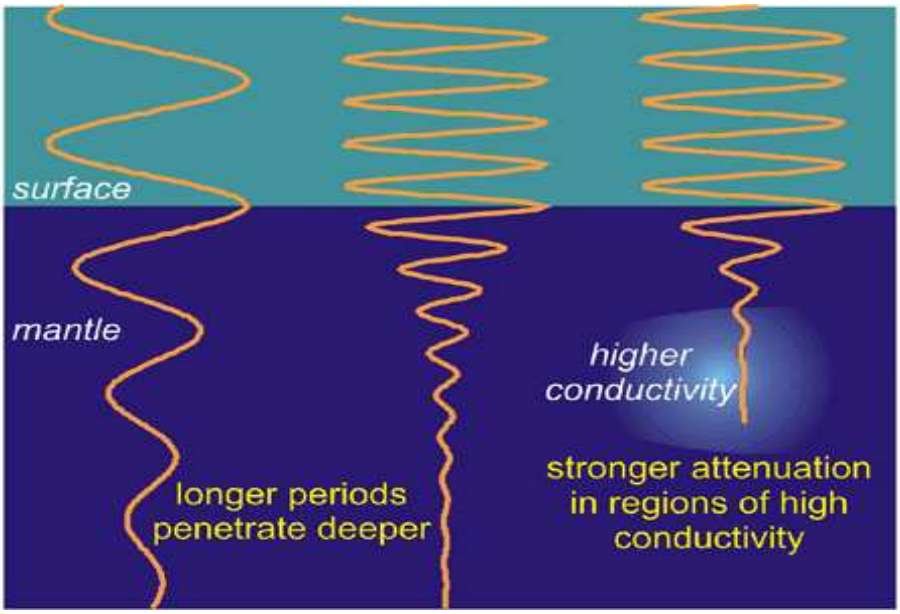

Figure 2.2: Depiction of signal penetration at different periods. Image courtesy of http://www.spacecenter.dk/research/solarphysics/electromagnetic-induction-studies

decreases the GIC magnitudes (Pirjola, 2000). It is important to note that the magnitude of the GIC in the conductors also depends on the network resistances and topology.

The plane wave model described in section 2.3.3 is applicable with a uniform conductivity model. For a layered Earth, eqn. (2.2) can be generalised. The assumption of a vertically propagated primary source field with single frequency still holds for the relation between E_y and B_x. The conductivity σ now takes the form of a frequency-dependent apparent conductivity (Pirjola, 2002c,b).

2.4 Computation of network coefficients and the GIC

The determination of the Earth's conductivity and subsequent modelling of the geoelectric field as discussed in Section 2.3.3 completes the geophysical aspect. The computation of the GIC from the modelled geoelectric field and the network coefficients constitutes the engineering aspect. There is a need to apply Ohm's

and Kirchhoff's laws and Thévenin's theorem on the power network in order to determine the power transmission network coefficients (Pirjola, 2002b). To carry out this step, an accurate description of the electrical power network configuration, the geometry and resistances (hereafter called system parameters) must be available. This is a purely engineering task and out of the scope of this study. For some details regarding this process, see Lehtinen and Pirjola (1985), Viljanen and Pirjola (1994), and references therein.

Power network configurations change over time as power companies expand their grids, thereby increasing the complexity of determining network coefficients. System parameters must be redefined each time there is a change on the network. However, Pulkkinen *et al.* (2007) have outlined a method which circumvents this complex process by using measured GIC and electric field or geomagnetic field data and where a knowledge of the system parameters is not necessarily required. Here, the latter method is presented which only requires a prior knowledge of one of the network coefficients. This method has been chosen because it utilises measured GIC and geomagnetic data as input parameters. The geoelectric field is a modelled parameter in GIC studies and would therefore not be an ideal input parameter for optimal modelling.

If we assume a spatially constant electric field and the network coefficients are known, then the GIC can be modelled by the equation

$$GIC\,(t) = a\,E_x\,(t) + b\,E_y\,(t) \tag{2.13}$$

where a and b are the network coefficients specific to each transformer and power line depending only on the resistance and geometrical composition of a power system (Viljanen and Pirjola, 1994). Note that in practice there is always some noise in the data but here the noise term has been neglected for reasons that will become clear later. The a and b parameters are given in units of A km/V if the electric field is given in units of V/km.

Taking the spectral form of eqn. (2.13) with the electric field expressed in terms of eqn. (2.7) where the horizontal geomagnetic variations are assumed to be linear with respect to the x and y coordinate plane leads to

$$G\tilde{I}C = \frac{a}{\mu_0}\,\tilde{Z}\,\tilde{B}_y - \frac{b}{\mu_0}\,\tilde{Z}\,\tilde{B}_x + (a\,-\,b)\,\tilde{\epsilon}_1 + \tilde{\epsilon}_2 \tag{2.14}$$

where the tilde sign depicts quantities in the spectral domain and $\tilde{\epsilon_1}$ and $\tilde{\epsilon_2}$ are the noise term contributions from eqn. (2.7) and (2.13) respectively. Multiplying eqn. (2.14) by B_x^* and B_y^* yields

$$G\tilde{I}C\tilde{B}_x^* - \tilde{\epsilon}\,\tilde{B}_x^* = \frac{a}{\mu_0}\,\tilde{Z}\,\tilde{B}_y\tilde{B}_x^* - \frac{b}{\mu_0}\,\tilde{Z}\,\tilde{B}_x\tilde{B}_x^* \tag{2.15}$$

$$G\tilde{I}C\tilde{B}_y^* - \tilde{\epsilon}\,\tilde{B}_y^* = \frac{a}{\mu_0}\,\tilde{Z}\,\tilde{B}_y\tilde{B}_y^* - \frac{b}{\mu_0}\,\tilde{Z}\,\tilde{B}_x\tilde{B}_y^* \tag{2.16}$$

with the asterisk denoting complex conjugate terms and $\tilde{\epsilon}$ being the combined noise term. Solving eqn. (2.15) and (2.16) then gives

$$c \equiv \frac{b}{a} = \frac{\tilde{B}_y\tilde{B}_x^* - \chi|\tilde{B}_y|^2}{|\tilde{B}_x|^2 - \chi\tilde{B}_x\tilde{B}_y^*} \tag{2.17}$$

where

$$\chi = \frac{G\tilde{I}C\tilde{B}_x^* - \tilde{\epsilon}\tilde{B}_x^*}{G\tilde{I}C\tilde{B}_y^* - \tilde{\epsilon}\tilde{B}_y^*} \tag{2.18}$$

The term c is independent of frequency and thus can be determined in the temporal domain by applying stationary conditions on the signal and then using the cross-correlation theorem (Pulkkinen *et al.*, 2007). The ratio c can then be expressed as

$$c = \frac{< B_y\,B_x > -\hat{\chi}\ < B_y\,B_y >}{< B_x\,B_x > -\hat{\chi}\ < B_x\,B_y >} \tag{2.19}$$

where

$$\hat{\chi} = \frac{< GIC\,B_x >}{< GIC\,B_y >} \tag{2.20}$$

with the terms $< ... >$ used as a representation of the expectation values. Statistically the noise term $\tilde{\epsilon}$ is assumed to be independent of B_x and B_y and has a zero mean. Thus the terms containing the combined noise do not appear in eqn. (2.19) and (2.20). Pulkkinen *et al.* (2007) argues that even though this simplification may not always hold true, the methods applied in this case have been seen to improve the modelling accuracy of GICs. Note from eqn. (2.17) that a knowledge of at least one network coefficient is required. However, this is much simpler than

the full process used in previous studies (e.g. Viljanen and Pirjola, 1994; Koen, 2002).

2.5 Summary

The Sun is the primary driver of space weather. Space weather activity follows approximately the 11-year sunspot cycle with a peak around solar maximum. During solar maximum there is an increase in the number of geomagnetic storms. The intensity of geomagnetic storms is determined by the interaction of the solar wind and the Earth's magnetic field which in turn is determined by the composition of the solar wind parameters.

Rapid changes in the Earth's surface magnetic field due to geomagnetic storms, induce an electric field at the Earth which gives rise to GICs in earth conductors. The plane wave model is the simplest model used in the modelling of the geoelectric field which is used as an input parameter for the calculation of the GICs. Figure 2.3 is a summary of the space weather chain of events leading to GICs. The magnitude of GICs in a power network is determined by magnetospheric-ionospheric currents, the ground conductivity and the system parameters.

Methods of deriving both a layered ground conductivity model and the network coefficients from a set of GIC and geomagnetic data have been reviewed. The ground conductivity is very important in the modelling of the geoelectric field, which together with the network coefficients determined using the system parameters, are used in the computation of the GICs. The new network coefficients and the derived ground conductivity model are discussed in the next chapter.

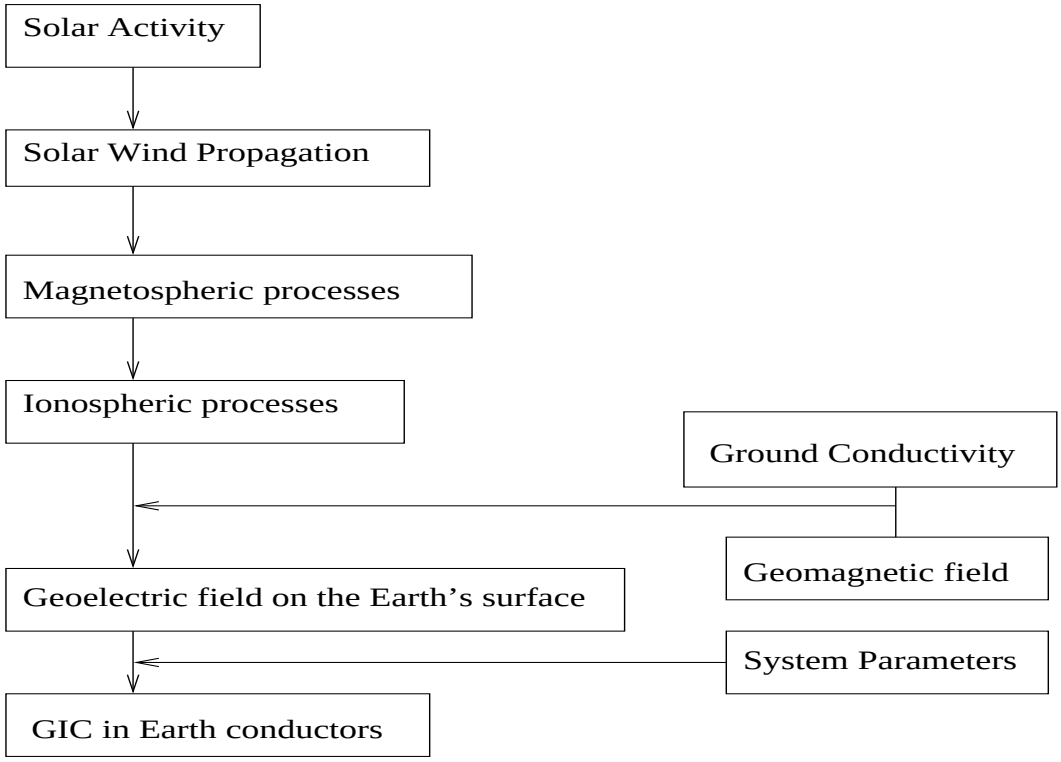

Figure 2.3: Space weather chain of events for GIC (a modified version of the Figure by Pirjola (2000)).

Chapter 3

Improving the modelling of GICs

3.1 Introduction

In efforts to model GICs in the Southern African power network, Koen (2002), Zatjirua (2005) and Bernhardi (2006) used a uniform one layer ground conductivity structure following ideas proposed by Viljanen and Pirjola (1994) and Pulkkinen (2003). Shortcomings in the uniform ground model can be compensated for by using a multilayered conductivity model that includes a wider frequency band associated with the GIC phenomena (Trichtchenko and Boteler, 2006; Pulkkinen *et al.*, 2007).

Koen (2002) also used methods by Lehtinen and Pirjola (1985) to determine the network coefficients a and b given in eqn. (2.13). These methods require a knowledge of the electrical power substation system parameters. In most cases, this information is not available and thus the task of updating the network coefficients as the system parameters change over time becomes almost impossible. However, Pulkkinen *et al.* (2007) have shown that measured GIC and geomagnetic field data can be used to update the network coefficients and that a knowledge of system parameters is not necessarily required.

In this chapter, a new set of network coefficients which were used in the derivation of the multilayered conductivity model are presented. The derived multilayered conductivity model is introduced and it is established that this model improves the accuracy of GIC modelling. It is then demonstrated that the derived multilay-

ered conductivity model degrades with increasing distance from the geomagnetic observatory and that it is valid only for the specific geomagnetic observatory and GIC station pair. A statistical analysis of the occurrence of GICs in the network which is based on model GIC values resulting from the new ground conductivity model and network coefficients is then carried out.

3.2 Determination of network coefficients

Power network configurations change over time, which in turn will also change the network coefficients. To take this into consideration, a new set of network coefficients which are then used as inputs for the multilayered conductivity model derivation have to be determined.

Koen (2002) modelled the GIC using a uniform resistivity of 1000 Ωm with network coefficients $a = -80\,\mathrm{A\,km/V}$ and $b = 15\,\mathrm{A\,km/V}$. By using the Hermanus geomagnetic field time derivatives and Grassridge measured GIC data for the period 29-31 October, 2003, the ratio c given by eqn. (2.19) was determined to be $c = -0.01$. The time derivatives of the geomagnetic field were used because of their characteristic shorter correlation time and approximately exponential decaying functional form (Pulkkinen *et al.*, 2007). Note that to use the ratio c to redetermine the network coefficients by eqn. (2.17) requires a knowledge of any one of the network coefficients. An arbitrary choice was made to keep the value of the coefficient a the same as Koen (2002) and then modify the coefficient b. The values for the new set are $a = -80\,\mathrm{A\,km/V}$ and $b = 1\,\mathrm{A\,km/V}$. The reason for the difference between the value of b as derived by Koen (2002) and the value presented here is not perfectly clear. One possible reason is that the non-1D nature of the true conductivity structure is partially captured by the derived coefficients. Whatever the reason for the difference, the fact remains that the derived coefficients give much better data-model agreement. Then, the new coefficients were used as input parameters for the multilayered conductivity model derivation. The first 12 hours of the data set was excluded in both network coefficients and conductivity model derivation and reserved for the model validation process carried out in Section 3.3.

According to Koen's (2002) coefficients the ratio c is $c = -0.19$, while that of

the new coefficients which are based on Hermanus data with a distance of 590 km from the GIC site is $c = -0.01$. There is significant a difference between the two ratios as also noted for the coefficient b above. To determine how quickly the ratio c changes with increasing distance from the geomagnetic observation site, data from Hartebeesthoek and Tsumeb having distances of 892 and 1759 km from the GIC site respectively, were included in the investigation. The resulting values of c are 0.132 and -0.103 for Hartebeesthoek and Tsumeb respectively. The Hartebeesthoek value differs considerablely from Koen's value. The value obtained for Tsumeb is unexpectedly close to Koen's value considering the distance from the GIC site. Reasons for this behaviour are a matter for future investigation.

3.3 Layered ground conductivity model

First, by applying the weighted least squares method given by eqn. (2.10), 1-minute mean geomagnetic field and GIC data and the new network coefficients were used

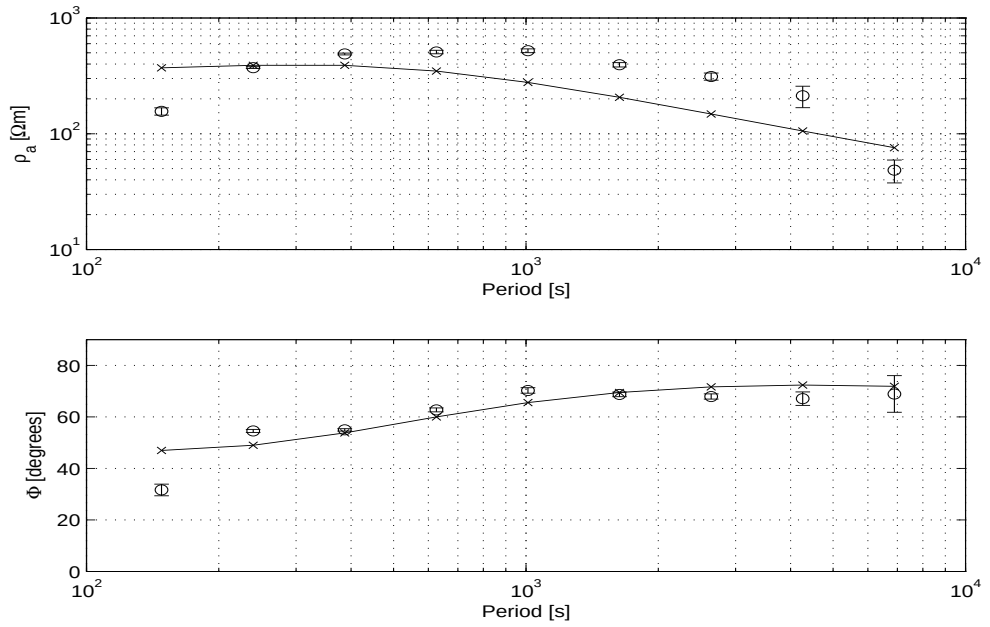

Figure 3.1: Circles: The apparent resistivity (top panel) and the phase (bottom panel) computed from the derived surface impedance. Crosses: The apparent resistivity and phase of the derived conductivity model.

to derive the surface impedance. Using eqn. (2.11) the apparent resistivities and the phases were computed from the derived surface impedance and are presented in Figure 3.1. It is seen from Figure 3.1 that despite the very limited amount of available data, a relatively good estimate of the surface impedance is obtained up to a period of about 7000 s. The smooth and continuous decrease in resistivity, with the phase remaining above 45° noted in Figure 3.1, is consistent with MT methods and allows for the determination of thickness of each layer (Simpson and Bahr, 2005, Chapter 2).

The surface impedance was then utilised in the simplified Occam's inversion algorithm used by Pulkkinen *et al.* (2007) to derive a 1-D 10-layer ground conductivity model (hereafter called layered ground model). The number of layers was chosen so as to minimise the complexity of the model while still capturing the central features in the vertical variations of the conductivity. The resulting conductivity model is shown in Figure 3.2 and the corresponding apparent resistivities and phases agree quite well with the values obtained from the derived surface impedance, as seen

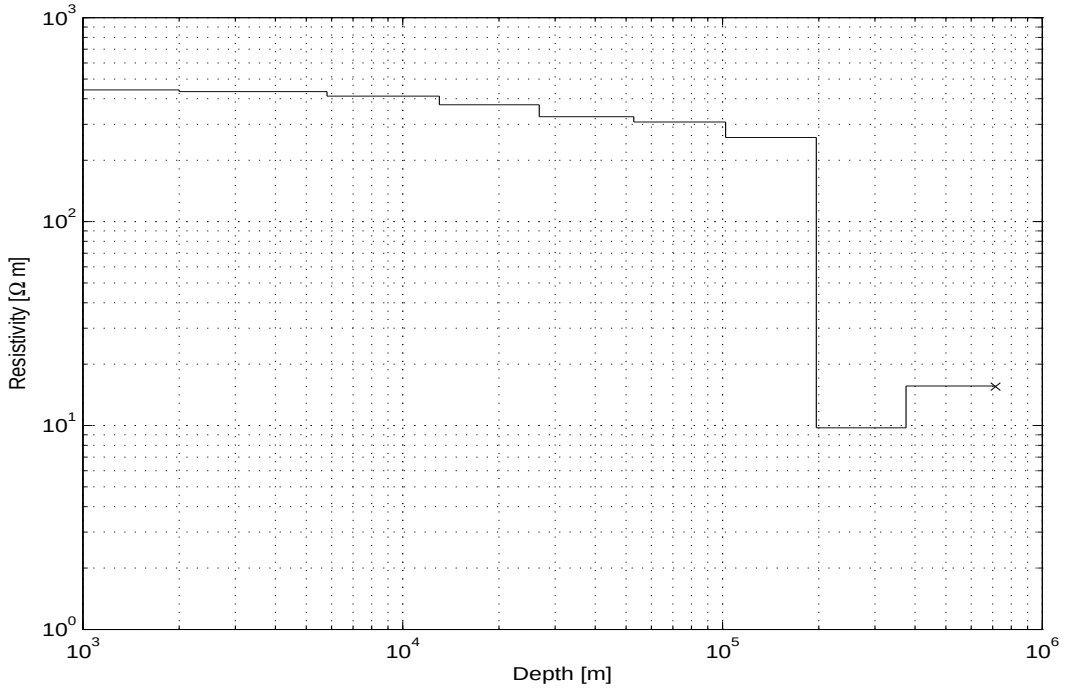

Figure 3.2: Ground conductivity model derived from the surface impedance. The cross denotes the resistivity of the terminating half-space.

Table 3.1: Derived resistivity values and corresponding layer thicknesses.

Layer Number	Resistivity[Ωm]	Layer thickness [km]
1	442	2.00
2	434	3.80
3	412	7.22
4	374	13.70
5	327	26.10
6	308	49.50
7	258	94.10
8	9.74	179
9	15.60	340
10	15.50	Infinite

in Figure 3.1. Table 3.1 shows the resistivity and corresponding layer thickness values of the derived conductivity model.

It should be noted that although the conductivity model in Figure 3.2 reflects the geological conditions of the region, there is a likelihood that it is not a very good characterisation of the actual conductivity and geological structure of the region. More specifically, the actual conductivity structure of Southern Africa is known to have strong lateral gradients rendering the ground very inhomogeneous (Hamilton *et al.*, 2006; Weckmann *et al.*, 2007). Thus, for example, the well-conducting layer at a depth of about 200 km seen in Figure 3.2 may be due to inhomogeneities rather than due to a true conductor in the lower crust or upper mantle (Constable, 1985). Since the goal of this work is not geological interpretation of the data, but rather the generation of an optimal model for the modelling of GIC events, any possible ambiguity associated with the interpretation of the derived layered ground model is not important. In any case, one should be careful to note that due to the inhomogeneous character of the actual ground, the layered ground model is most likely to be valid only for the specific geomagnetic observatory and GIC station pair used and should be applied with caution to any other situations as shown in the next section.

3.4 Analysis of the layered ground model and network coefficient

The geoelectric field is modelled by the plane wave method using Hermanus magnetic field data and the layered ground conductivity model. The GIC is first computed using eqn. (2.13) with the uniform ground model and network coefficients of Koen (2002), and then with the layered ground model and new network coefficients. The validity of the layered ground model and new network coefficients is then tested by making a comparison of the two model GIC computations to the measured GIC for the Halloween storm event of October 29, 2003. The data set for the first 12 hours of October 29, which was not used in the derivation process,

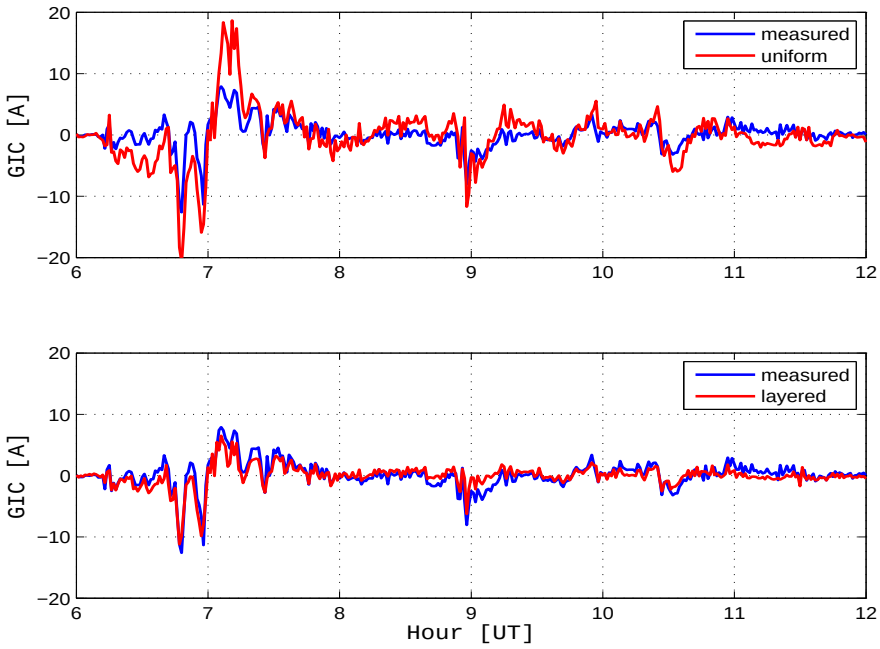

Figure 3.3: A comparison of the modelled GIC with the measured GIC using two different ground models and network coefficient sets for the Halloween storm of 29 October, 2003. Top: GIC modelled using network coefficients and uniform ground model by Koen (2002). Bottom: GIC modelled using layered ground model and new network coefficients. The interval shown was not used in the derivation of the new network coefficients or the layered conductivity model.

was used in this test and the results are shown in Figure 3.3. Clearly, the layered ground model and new network coefficients produce a much more accurate representation of the event. It is interesting to note that although the uniform model manages to represent all the interesting features seen in Figure 3.3, there is a gross overestimation of the peaks, particularly between the hours 06:00 to 07:00 and 07:00 to 08:00 UT.

The difference between measured and modelled GIC values was determined and the error distribution derived is given in Figure 3.4. The distribution shows that the layered ground model and new network coefficients effectively reduce the number of large errors. Relative errors defined as $(\mathrm{GIC}_{measured} - \mathrm{GIC}_{modelled})/\mathrm{GIC}_{measured}$ were computed for GIC values corresponding to $|\mathrm{GIC}_{measured}| > 1$ A. The median error for the layered model is 48 % while that for the uniform layer model is 82 %.

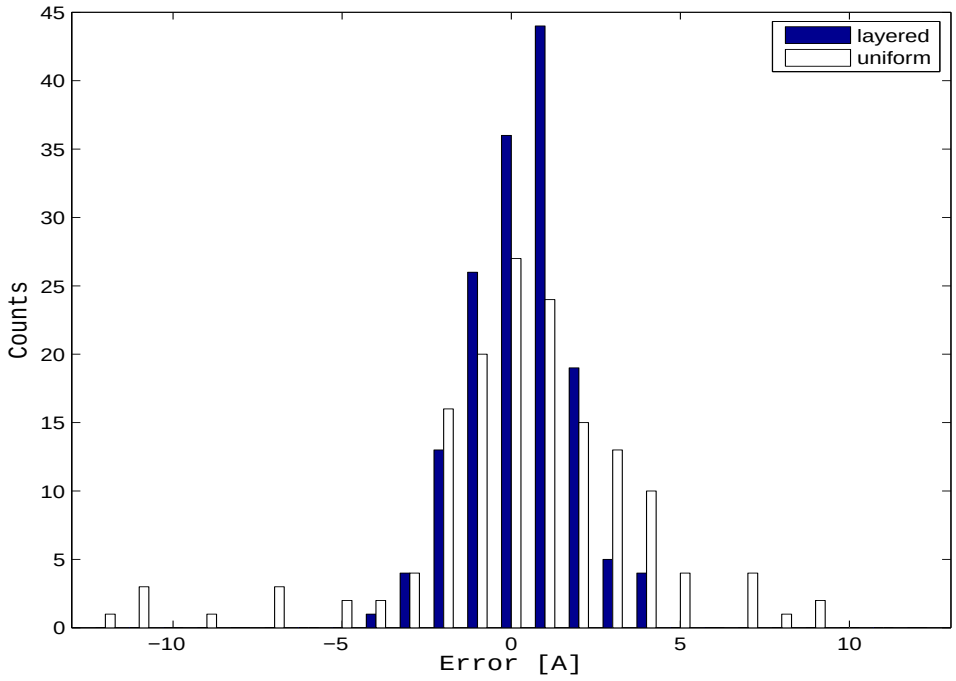

Figure 3.4: Error distribution defined by $(\mathrm{GIC}_{measured} - \mathrm{GIC}_{modelled})$. White bars show distribution of GIC modelled using network coefficients and ground model by Koen (2002) and blue bars show the distribution of GIC modelled using ground model and network coefficients derived here. A bin width of 1 A was used.

The root mean square deviation (RMSD) defined as

$$\left(\sum_{i=1}^{n}(GIC_{measured,i} - GIC_{modelled,i})^2/n\right)^{1/2}$$

was also determined for the two models. The RMSD method is used to compare the deviation of two models with respect to the measured data set. This is achieved by aggregating the individual differences into a single measure of predictive power, with positive values close to zero indicating an accurately modelled GIC. The layered ground model and network coefficients show a good improve-

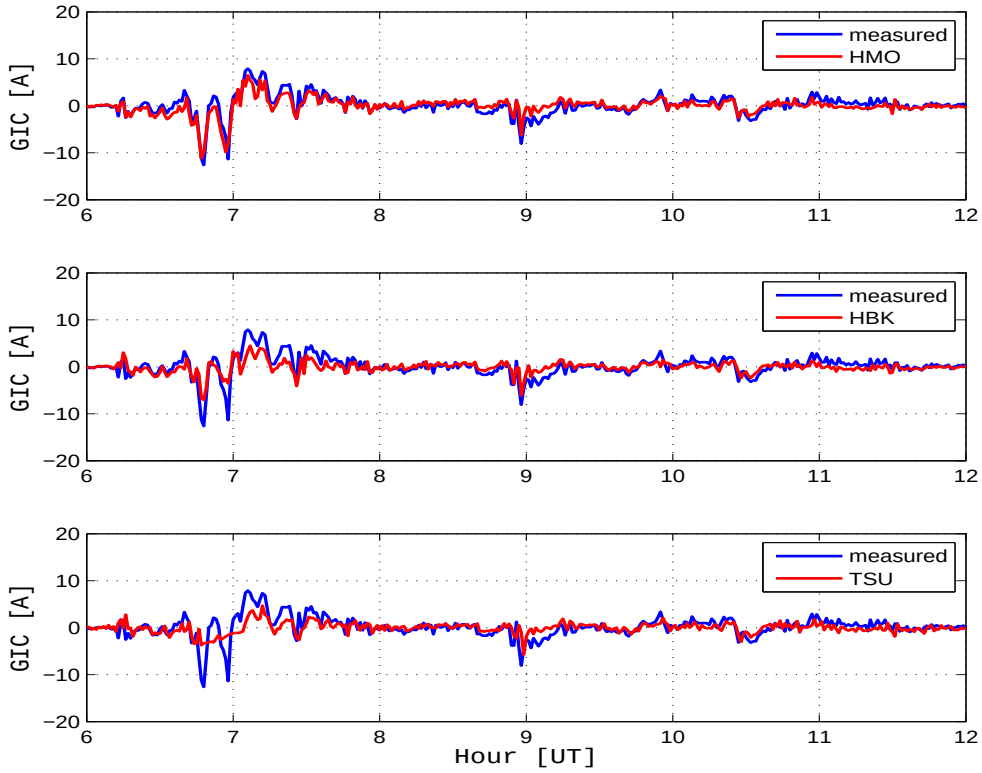

Figure 3.5: A comparison of the modelled GIC to the measured GIC using the layered ground model and new network coefficients for the Halloween storm of 29 October, 2003. Top: GIC modelled using Hermanus geomagnetic field data as in Figure 3.3. Middle: GIC modelled using Hartebeesthoek geomagnetic field data. Bottom: GIC modelled using Tsumeb geomagnetic field data. The interval shown was not used in the derivation of the new network coefficients or the layered conductivity model.

ment with a RMSD value of 1.56 compared to the value of 3.49 for the model with uniform ground.

Most of the geomagnetic observation sites in Southern Africa are very far from the GIC sites. It was previously stated that the new ground model should be used with caution as it may not work well with other data apart from Hermanus data. The applicability of the layered ground model to other geomagnetic observatory data was tested by using Hartebeesthoek and Tsumeb geomagnetic data. The results are given in Figure 3.5. The distances of the two geomagnetic stations from the GIC site are 892 and 1759 km respectively. The performance of the two data sets degrades with increasing distance from the geomagnetic station. Particularly notable in Figure 3.5 is the failure of the two data sets to efficiently represent the amplitude of the GIC peaks seen between the hours 06:00 to 07:00 and 07:00 to 08:00 UT, which are important in GIC studies. The median errors for Hartebeesthoek and Tsumeb distributions are 64 % and 74 % with RMSD values of 2.21 and 2.73 respectively, which agree with the observations given in Figure 3.5.

3.5 Discussion

Network coefficients are critical in the modelling of GIC events. The method used here to derive the new network coefficients is very simple and circumvents the complex process associated with the full GIC modelling of the system that would require knowledge about the system parameters of the entire power grid. There are changes in the ratio c with increasing distance of the geomagnetic observatory from the GIC site for some sites such as Hermanus and Hartebeesthoek, but the results obtained for Tsumeb require further investigation before a conclusion can be drawn.

The layered ground model and the new network coefficients are seen to improve the accuracy of GIC modelling. To get more reliable results would require additional GIC data. It is argued that the new model could perform much better than the 48 % relative error found in the analysis, if a larger data set would be available for the derivation process. Pulkkinen *et al.* (2007) used a sample space with 8 days of

data and their results yielded a relative error of 35 %.

When considering the layered ground conductivity model, one should note that it does not take into account the important lateral variations in the conductivity structure such as the continent-ocean boundaries. Southern Africa is known to have electrical ground conductivity anomalies (Constable, 1985; Hamilton *et al.*, 2006; Weckmann *et al.*, 2007) and thus this ground model is only applicable to the Grassridge station until further studies on conductivity structures have been carried out at other GIC sites. Further, the layered ground model degrades with increasing distance between the geomagnetic observatory and the GIC site as shown in Figure 3.5. It is thus important to use geomagnetic observatory data nearer to the GIC site as explained by Viljanen *et al.* (2004). This implies, that to achieve maximum efficiency required for GIC modelling, the layered ground model is best applicable for the Grassridge substation with Hermanus geomagnetic data.

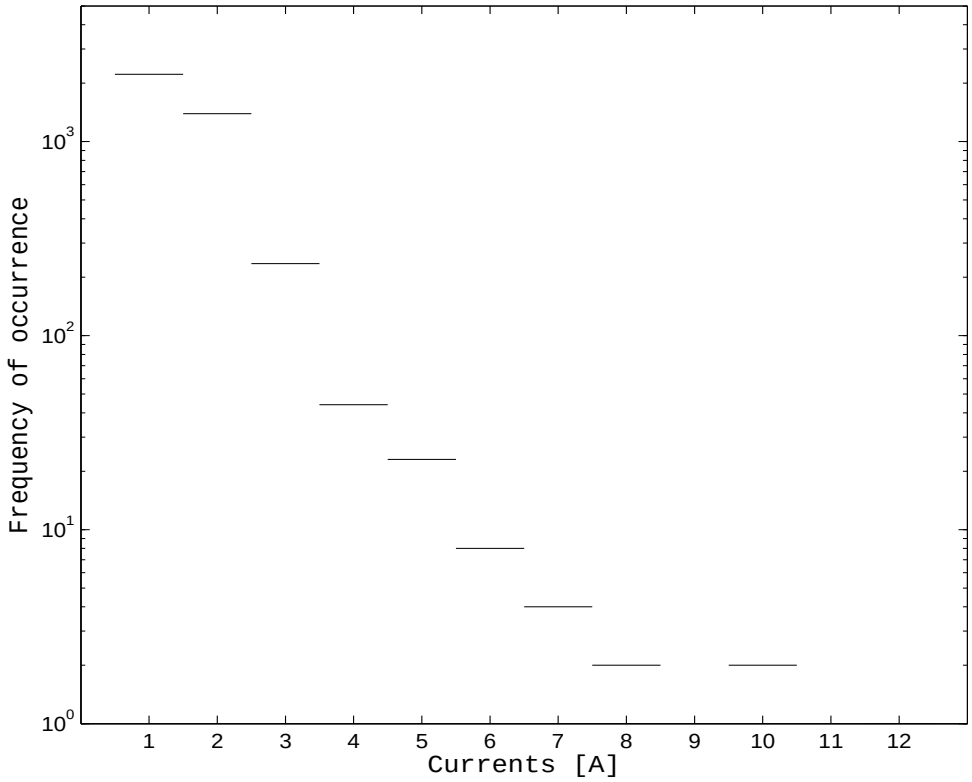

Figure 3.6: GIC statistics for period 1996-2006 based on absolute GIC magnitude > 1 A.

Based on the layered ground model, the new network coefficients and geomagnetic field measurements at Hermanus, model GICs were computed for 86 geomagnetic storm events, assuming that the network is the same as used in the surface impedance derivation during the period 1996-2006. Then a statistical estimation of the occurrence of $|\,\mathrm{GIC}\,| > 1$ A in the power system was conducted and the results are shown in Figure 3.6 for Grassridge. Currents seen here are much smaller than those observed at higher latitudes like in Finland where currents as much as 57 A were measured during the October 2003 events with no reported transformer failures (Viljanen *et al.*, 2006). The largest absolute GIC value within the period of interest was 11.9 A and occurred during the 29 October 2003 geomagnetic storm, while the largest measured GIC value for the said storm was 12.6 A.

Considering the level of currents shown in Figure 3.6, it is clear that the South African network is at risk. To experience transformer failures even at such low GIC amplitudes could probably be related to the design of the transformers as reported by Viljanen and Pirjola (1994) and Pirjola (2000), or to the design of the power system as a whole. There is a need to carry out an investigation to determine which of the two cases is more responsible for the failures. Nowadays, there are many interconnected power systems spanning large geographical areas which may suffer from a shortage of volt-ampere reactive power. This is very prominent during heavy system loading and may lead to voltage collapse of the system and extensive blackouts (Kappenman *et al.*, 2000; Molinski, 2002). Kappenman *et al.* (2000) states that the effects of space weather can create large-scale problems because the footprints of a magnetic storm can extend over a large area and cause simultaneous widespread stress in a power grid which can result in widespread failures across a region.

The work presented in this chapter is part of a manuscript that has been submitted for publication to Space Weather Journal.

Ngwira C. M., A. Pulkkinen, L. A. McKinnell and P. J. Cilliers, Improved modeling of geomagnetically induced currents in the South African power network, *Manuscript submitted to the Space Weather Journal*, April 2008.

Chapter 4

Characterising the GICs

4.1 Introduction

Intense geomagnetic activities are known to give rise to large GIC events on power transmission grids (Pirjola, 1983, and references therein). In order to characterise GIC events, it is important to understand the related parameters.

This chapter looks at the different properties of the geomagnetic field components, their time derivatives and some local geomagnetic indices used for GIC monitoring. The immediate goal of this work is to determine which parameters can be used to assess the severity of any given geomagnetic storm and the future goal is to use the determined parameters to make classifications of the local storm conditions and relate them to the expected GIC levels in the power system. Classification is very important in the forecasting of GICs and is widely used by power system operators to monitor geomagnetic related activity in the power system (Trichtchenko and Boteler, 2004; Kappenman, 2005; Thomson *et al.*, 2005; Viljanen *et al.*, 2006).

To carry out the investigations 86 geomagnetic storm events were selected based on a geomagnetic K-index value greater than 5 as derived from observations at Hermanus, South Africa. Data from 1996 to 2006 with a 1-minute sampling interval was used. The rate of change of the geomagnetic field was determined by taking the difference between two successive values and then dividing by the sampling interval. In order to make comparisons between any given geomagnetic index and the GIC, model GIC data for the Grassridge substation was used due to data limitations

highlighted in Chapter 1.4. The model GIC was computed using eqn. (2.13) with the new network coefficients and layered ground conductivity model introduced in Chapter 3. Hermanus geomagnetic field data was used. It was assumed that the system parameters were constant during the entire period under consideration.

4.2 Geomagnetic field and its time derivatives

The geomagnetic field (**B**-field) is measured at different geomagnetic observatories around the world. The observed geomagnetic field depends on the ionospheric-magnetospheric primary source currents (Viljanen and Pirjola, 1994). From a modelling point of view, the horizontal geoelectric field is the key parameter that must be determined accurately. The calculated geoelectric field, which was used as an input for the computation of GICs according to eqn. (2.13), relates more to the geomagnetic field rate of change than the geomagnetic field (Viljanen *et al.*,

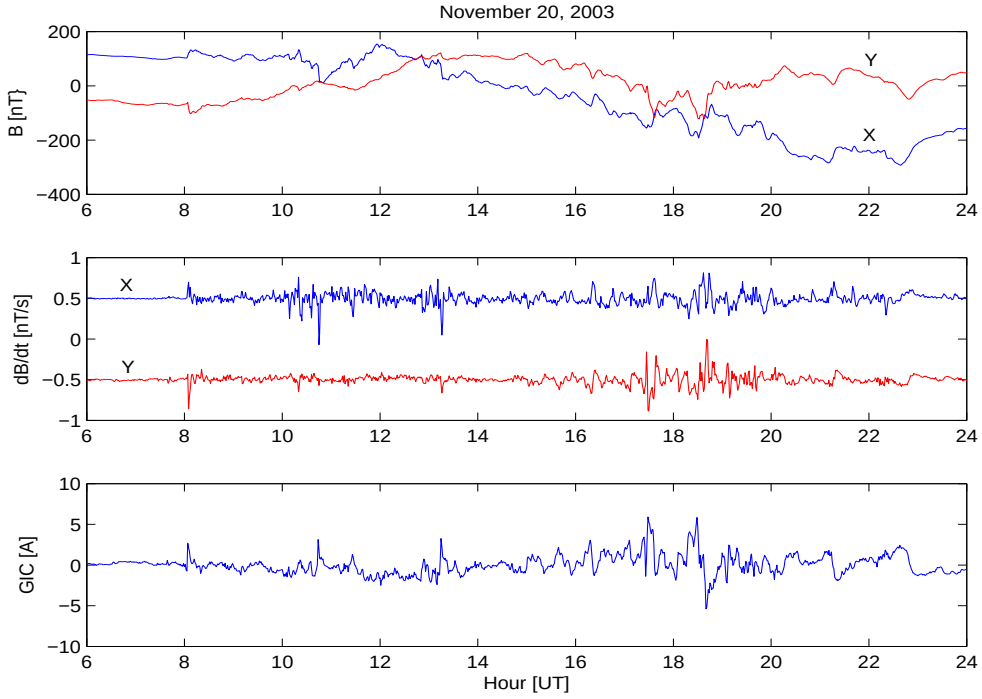

Figure 4.1: The horizontal geomagnetic field (top panel), time derivatives of the X (north-directed) and Y (east-directed) components (middle panel) and the model GIC (bottom panel) based on Hermanus geomagnetic data.

2006). Viljanen and Pirjola (1994) report that because the geoelectric field is not often measured, the rate of change in the horizontal geomagnetic field is used as it is related to the geoelectric field by eqn. (2.3).

The rate of change of the geomagnetic field is closely related to the GIC (Viljanen *et al.*, 2001; Kataoka and Pulkkinen, 2008, and references therein). An analysis of the maximum rate of change for each individual geomagnetic event under consideration shows that the magnitudes of the peaks of dX/dt, dY/dt and dZ/dt are comparable. For dZ/dt to be comparable to dX/dt and dY/dt suggests the existence of coastal effects which are known to strongly influence the Z component for observatories near the ocean-continental boundary like Hermanus Magnetic Observatory. It must be pointed out that only the horizontal components X and Y are used in the modelling of GICs, as established by eqn. (2.13). Plotted in Figure 4.1 are the B-field horizontal components X and Y, their time derivatives dX/dt and dY/dt and the model GIC for the November 20, 2003 storm. Figure

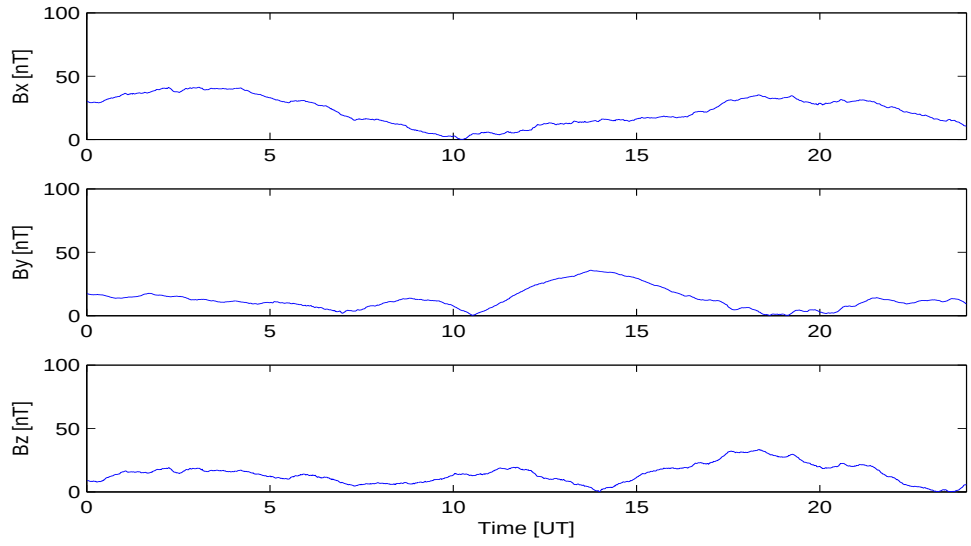

Figure 4.2: Diurnal variation of the geomagnetic B-field components X, Y and Z averaged over 86 storm days during the period 1996-2006 at Hermanus, with a 1-minute sampling interval. The South African standard time is about UT+2 hours.

4.1 shows that the pattern of the GIC variations (bottom panel) relates closely to that of the horizontal rate of change (middle panel). Viljanen (1997) explains that the geophysical processes involving GICs are very complex by highlighting instances when the GIC peaks were equal, but the geomagnetic X and Y and the time derivatives dX/dt and dY/dt were different at those instances. This has been attributed to small-scale currents causing large time derivatives.

Figure 4.2 depicts the diurnal variation of the geomagnetic field components averaged over the 86 geomagnetically disturbed days. The diurnal variation for each component is different from the others. For instance, the peak seen at 20:00 UT in the X component is a minimum for the Y component. Illustrated in Figure 4.3 is the average diurnal variation for the rate of change components. The same trend is noted where the diurnal variations of the components differ. Figure 4.2 and 4.3 clearly establish that the diurnal variation of the geomagnetic field and its time derivatives do not have a one-to-one relation. One should note that for monitoring

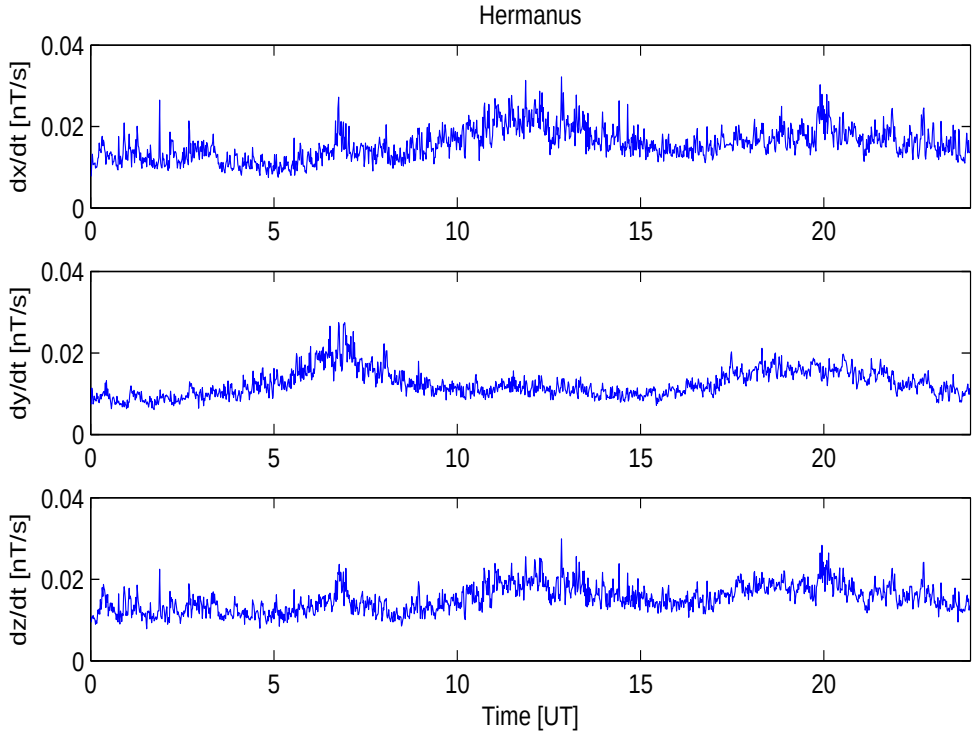

Figure 4.3: Diurnal variation of the rate of change of the geomagnetic field averaged for the same 86 storm events of Figure 4.2.

purposes, it is ideal to consider both components of the horizontal field as the geoelectric field can be large in any direction. Further, it should be mentioned that large GICs can occur at any time of the day and not only during the peak hours observed in Figure 4.2 and 4.3.

An investigation was carried out comparing the variations of the rate of change in the horizontal field dH/dt and its components dX/dt and dY/dt for a number of geomagnetic events at Hermanus, Hartebeesthoek and Tsumeb. Shown in Figure 4.4 is a comparison of dH/dt and the variations in dX/dt and dY/dt components for the July 25, 2004 geomagnetic storm event at Tsumeb. Figure 4.4 and other data not shown here, show that the variations in the dH/dt component generally follow more closely those in the dX/dt component than the dY/dt component. However, the true directional preference of the horizontal geomagnetic field rate of change is a matter that should be further investigated in the future using approaches similar to those of Boteler *et al.* (1994), Viljanen *et al.* (2001) and Trichtchenko and Boteler (2004).

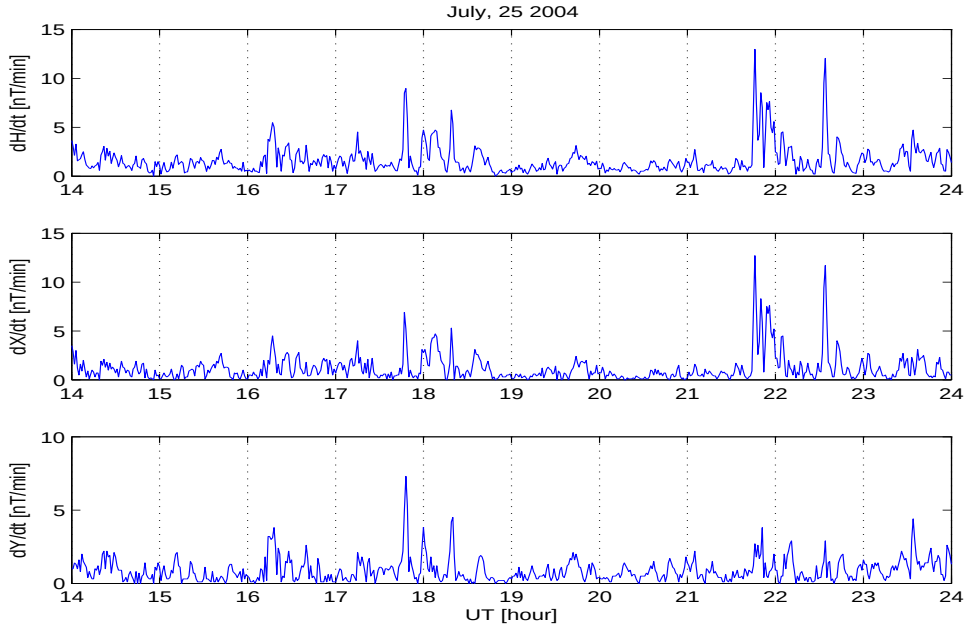

Figure 4.4: Comparison of the time derivative of the horizontal geomagnetic field dH/dt and its components dX/dt and dY/dt for Tsumeb.

The geoelectric field at the surface of the Earth is the key parameter for the calculation of the GICs. A rotation of the horizontal geomagnetic field rate of change by approximately 90° anticlockwise is a proxy for the corresponding geoelectric field (Viljanen *et al.*, 2001). The proxy is a consequence of Maxwell's curl equation introduced in eqn. (2.1). Figure 4.5 is a plot of the geoelectric field x and y components and the GIC during the storm of October 29-30, 2003 derived using the layered ground model with Hermanus geomagnetic data. It is interesting to note that the E_x component, which corresponds to the horizontal rate of change component dY/dt, appears to be an almost inverse plot of the GIC. This observation agrees with the north-south orientation of the power line feeding into the transformer at Grassridge. The geoelectric field includes the induction effects of the Earth which are not taken into account when considering the geomagnetic field rate of change (Viljanen *et al.*, 2001; Trichtchenko and Boteler, 2004, and references therein).

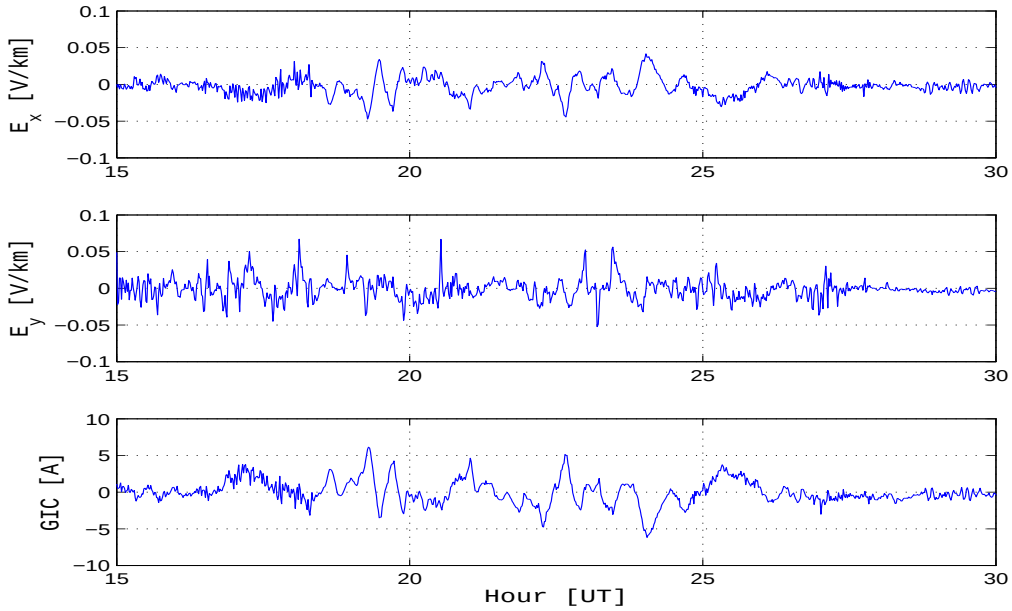

Figure 4.5: The geoelectric field components E_x and E_y determined using Hermanus geomagnetic data compared to the measured GIC data for the geomagnetic event of 29-30 October 2003.

4.3 The K-index as severity index

The K-index is the most widely used geomagnetic index for classifying the level of local 3 hour geomagnetic activity. Figure 4.6 shows the frequency of occurrence of the various local K-index levels as determined from data recorded at Hermanus for the period 1996-2006. What is seen is that the frequency of occurrence of K ≥ 5, which is the lower limit for the selected storms is small and decreases as you move towards K = 9. Large GICs are usually associated with the severe storms of K ≥ 7. It is evident from Figure 4.6 that the occurrence of such events is very low, but that does not reduce the risk of high GIC levels in the network, as GICs are also dependent on the system parameters and the ground conductivity. The fact that severe geomagnetic events are present and have occurred shows that there is a potential for large GICs within the South African network conductors and, therefore, is a source of concern.

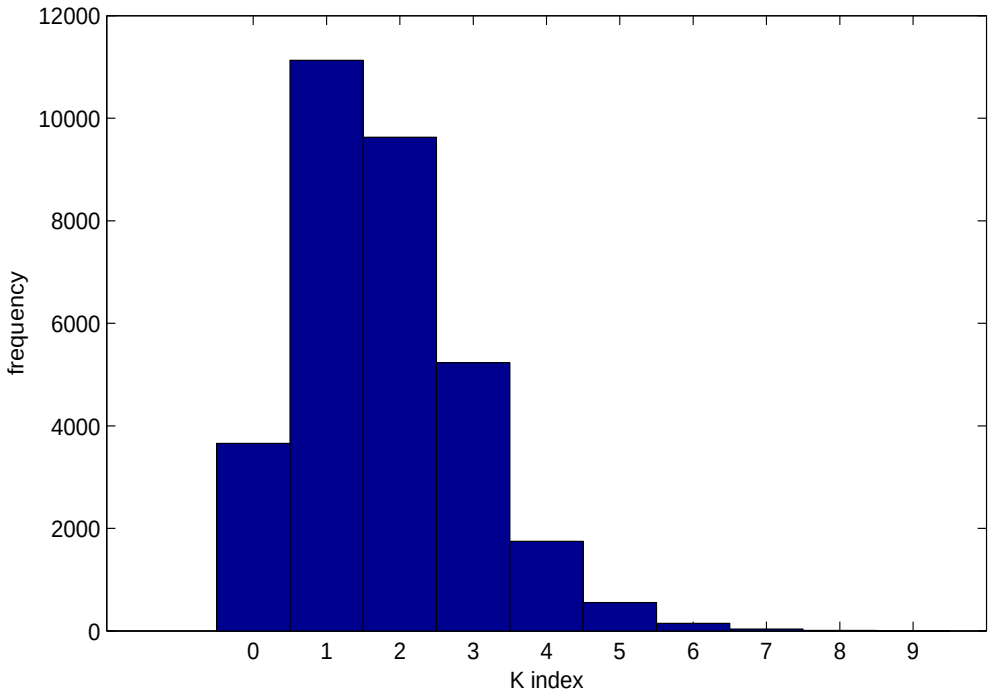

Figure 4.6: Frequency of occurrence of various K-index levels at Hermanus during the period 1996-2006.

Trichtchenko and Boteler (2004) established that there is a good correlation between the peak GIC and local geomagnetic indices. The magnitude of GICs is region dependent and one would assume that the local K-index would be a good indicator of the expected GIC levels in the regional power systems. Unfortunately, this is not the case, since the process of determining the K-index involves averaging, which severely blurs the important location and temporal characteristics of the geomagnetic storm (Kappenman, 2005). As a result, the K-index does not provide a well defined characterisation of possible dB/dt ranges which are necessary to characterise the level of GICs as the index approaches K= 9 (Kappenman, 2005). The major problem is that the index does not have an upper limit to categorise the expected dB/dt at the severe intensity of K = 9. Viljanen *et al.* (2006) inspected some geomagnetic storms that began with a sudden storm commencement and showed that a small B-field amplitude with rapid variations can produce a large dB/dt and high GIC levels. Knowing the expected value of dB/dt is very critical for power system GIC management, since large GICs can be induced within a short time. A forecast of K = 9 value is not a good indicator of potential effects of GICs for power system operators; a more helpful parameter would be the expected peak value of dB/dt or an estimation of the GIC levels (Kappenman, 2005; Viljanen *et al.*, 2006).

The task of estimating the expected GIC levels in a power system is very essential for power system management. Since the K-index has limitations, there is need for another index or indices that will provide a better indication of the GIC levels. Two indices in use for this purpose today are the geomagnetic range index, developed by Canadian geomagnetic observatories and the hourly standard deviation, developed by the British Geological Survey (BGS). The correlation between the GICs and these two indices are investigated separately in the following two sections.

4.4 Geomagnetic range indices

Trichtchenko and Boteler (2004) used both local and global geomagnetic indices in their study to determine the relationship between geomagnetic indices and the GICs. Their study showed that there is a better correlation between the GIC and local indices than between GIC and the global indices. Therefore, only local

indices were considered in this study because the interest is in local geomagnetic conditions which have a greater influence on the GIC amplitudes observed.

Geomagnetic range indices are used by Canadian geomagnetic observatories for monitoring and analysing GIC activities in technological systems such as power transmission and oil pipelines (Trichtchenko and Boteler, 2004). The determination of the range indices is done on an hourly basis. Trichtchenko and Boteler (2004) have shown that it is much easier to predict the envelope of the GIC variations (in this case the hourly envelope) than the actual detailed GIC variations (such as 1-minute values). The hourly range index (HRI) is determined by taking the difference between the maximum and minimum values during the hour. Alternative measures of local geomagnetic activity are determined by taking the maximum hourly value (MHV) of the geomagnetic field and the rate of change for the X and Y components. The GIC is closely related to the rate of change of the geomagnetic field and so the maximum observed value of the rate of change experienced by the field during an hour is an important indication of the expected GIC levels. The HRI and MHV of the rate of change are a good measure of the geomagnetic spectral power of the GIC (Trichtchenko and Boteler, 2006; Kataoka and Pulkkinen, 2008). Absolute values of the geomagnetic indices and the GIC are used. The amplitude of the currents cause saturation in transformers irrespective of the sign of the GICs (Pulkkinen, 2003; Trichtchenko and Boteler, 2004). Also included here are the hourly range index values for the GIC and the rate of change in the geomagnetic field.

Based on 86 geomagnetic disturbed days and model GIC data, an investigation of the two indices (i.e. HRI and MHV) was carried out with Hermanus geomagnetic data. An analysis was not done for Hartebeesthoek and Tsumeb because the model used for GIC computations gives better results with Hermanus geomagnetic data than with Hartebeesthoek and Tsumeb geomagnetic data, as shown in the previous chapter. To compare the GIC and the HRI or MHV, the data was binned into one-hour intervals each containing 60 data points. The maximum amplitude of the |GIC| and the corresponding index |HRI| or |MHV| were then obtained for each bin. The correlation coefficients (CCs) were determined using all the data points gathered from the individual storms. The comparisons were carried out as

Table 4.1: Summary of the correlation coefficients between GIC indices and geomagnetic indices based on the X and Y components and their time derivatives. 2064 data points were used in the investigation.

GIC	Geomagnetic index	X	Y	dX/dt	dY/dt
Max	Max	0.0044	0.0940	0.7208	0.8534
Max	HRI	0.8010	0.8367	0.7438	0.8583
HRI	HRI	0.8110	0.8210	0.7679	0.8944

follows: the maximums of the various components were compared to the peak GIC (Max-Max), then the peak GIC to hourly range (Max-HRI) and finally the hourly range GIC to the hourly range index of the components (HRI-HRI). A summary of the results is given in Table 4.1.

The CCs involving the Max-Max in the horizontal geomagnetic components X and Y are very low. This is to be expected since the horizontal geomagnetic components are not a good measure of the spectral power of the GIC. On the other hand, there is a good correlation for Max-HRI and HRI-HRI involving the horizontal components. Trichtchenko and Boteler (2006) explain that the HRI was designed to better capture the local geomagnetic variability. The results involving the time derivatives also have good CCs in all cases. The correlations involving HRI in the X component and the peak GIC (Max-HRI) are better than those of the Max-Max for the GIC and the rate of change dX/dt, and the opposite is true for the Y component. These results differ from those obtained by Kataoka and Pulkkinen (2008) who found that there was better correlation using the hourly peak rate of change rather than using hourly range values. The results of Kataoka and Pulkkinen (2008) agree well with results by Trichtchenko and Boteler (2004). However, the investigations by Kataoka and Pulkkinen (2008) were done for each storm phase. Also, the results here are based on model GIC data which may be the cause for these differences.

Generally, there is a higher correlation for the east-west components of the HRI and the rate of change to the GIC than for the north-south components as seen in Table 4.1. This is consistent with the north-south orientation of the power line feeding the transformer at Grassridge. Further, a check on the individual storms

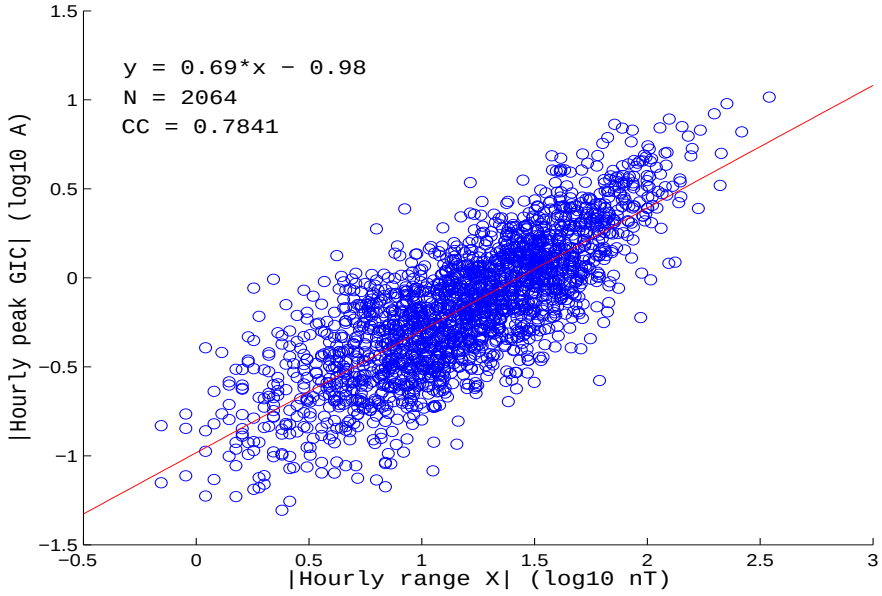

Figure 4.7: Scatter plots of the hourly peak GIC and the hourly range index for the X component at Hermanus. N is the number of data points in the set and CC is the correlation coefficient.

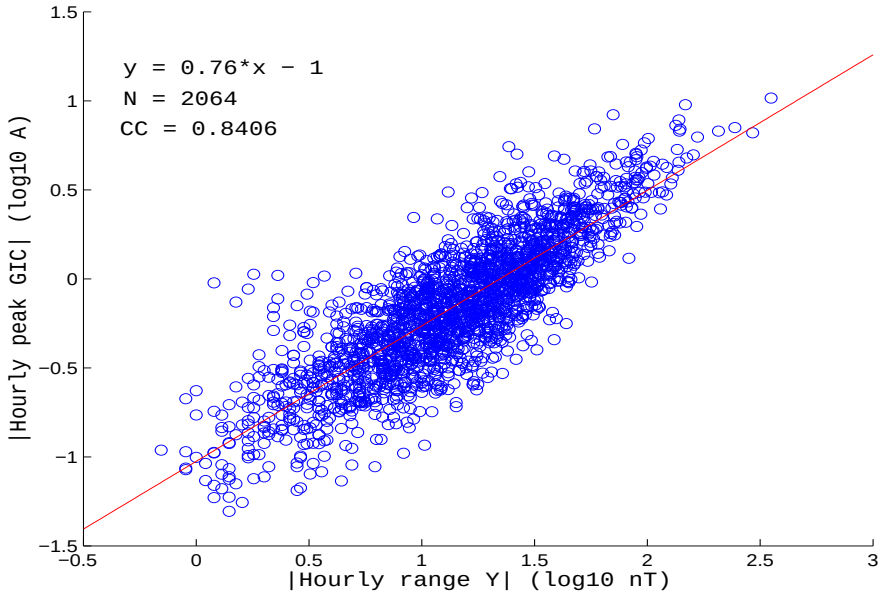

Figure 4.8: Scatter plots of the hourly peak GIC and the hourly range index for the Y component at Hermanus.

shows that there are certain events (about 20 %) where the correlation for dX/dt is better than that for dY/dt. Figure 4.7 and 4.8 are scatter plots of the hourly peak GIC with the hourly range index for X and Y. The two Figures show that the hourly peak GIC levels rarely exceed 10 A.

4.5 Hourly standard deviation

The instantaneous electric field at the Earth's surface does not merely depend on the instantaneous rate of change of the geomagnetic field, but on the integrated rate of change over a particular interval (Beamish *et al.*, 2002, and references therein). Beamish *et al.* (2002) argue that the maximum rate of change is not necessarily the best index to use as an indicator of the magnitude of the induced electric field. Beamish *et al.* (2002) also argue that the standard deviation in the horizontal geomagnetic field over a given interval in the time domain (in this case one hour) serves as an indicator of the total magnetic spectral power within that interval.

The hourly standard deviation (HSD) is an index that was developed by the BGS and is used by the Scottish Power company to monitor GIC activity on the Scottish power network (see Beamish *et al.*, 2002; McKay, 2003; Thomson *et al.*, 2005). The BGS monitoring service involves the provision of hourly geomagnetic activity indices from three magnetic observatories directly to the grid control centre for the Scottish power network. The monitoring system uses the HSD in the X and Y components of the geomagnetic field. The Scottish Power company monitors the level of DC currents flowing in the neutral points of main transmission transformers and the HSD is used by system operators to determine whether the observed DC increase is due to geomagnetic activity.

An analysis of the HSD was carried out using the horizontal geomagnetic components X and Y recorded at Hermanus. The correlation of the HSD with the model GIC was determined using the same data and methods highlighted in the previous section. The analysis was extended to include the time derivatives of the horizontal components. Results are shown in Table 4.2. The CCs for the various components exhibit similar trends to those exhibited by the HRI, where there is a

Table 4.2: Summary of the correlation coefficients between GIC indices and hourly standard deviation based on the X and Y components and their time derivatives using Hermanus data.

GIC	Geomagnetic index	X	Y	dX/dt	dY/dt
Max	HSD	0.6497	0.7564	0.7663	0.8875
HSD	HSD	0.6688	0.7766	0.7054	0.8544

higher correlation for the Y components than the X. Further, correlations between the peak GIC and the HSD (Max-HSD) are much lower than the correlations between the peak GIC and HRI (Max-HRI) for the X and Y components in Table 4.1. This observation implies that the HRI has a better spectral relation to the hourly peak GIC than the HSD.

The HSD analysis was extended to include Hartebeesthoek geomagnetic data in order to carry out a comparison between the Hermanus and Hartebeesthoek stations. To do this it was necessary to analyse the same number of geomagnetic storms. Due to bad or missing data for Hartebeesthoek 74 geomagnetically disturbed days were considered for the analysis that follows. A threshold of 15 nT was set so that only values exceeding this threshold were considered in the analysis of the diurnal, seasonal and solar cycle variations. The 15 nT threshold was decided upon because it was exceeded by at least 98 % of the geomagnetically disturbed days under consideration at both geomagnetic stations.

Figure 4.9 is a comparison of the diurnal variation at both Hermanus and Hartebeesthoek for the X and Y components of the HSD. The variations at both stations display a similar trend but are different for the X and Y components. A comparison of this diurnal variation with that derived for the geomagnetic field (B-field) and its time derivatives (presented in Figure 4.2 and 4.3 respectively), shows that there is a good agreement between the diurnal variation in Figure 4.9 and that for the time derivatives in Figure 4.3. Figure 4.9 shows peak activities around 20:00 and 22:00 hrs UT for the X and Y components respectively (South African standard time is 2 hrs ahead of UT).

The known tendency for geomagnetic activity to vary seasonally is clearly seen in

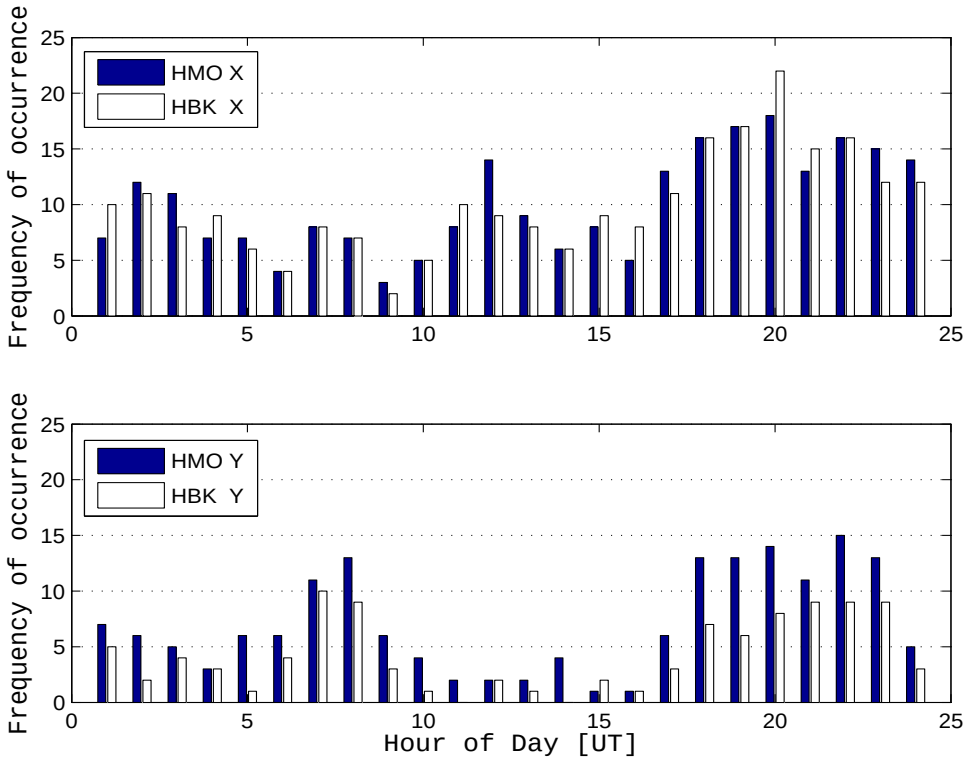

Figure 4.9: Comparison of the diurnal variation at Hermanus (HMO) and Hartebeesthoek (HBK) for the X and Y components of the HSD. Only HSD values greater than 15 nT were considered.

Figure 4.10. This is in agreement with the general increase in geomagnetic activity observed near the equinoxes (Viljanen *et al.*, 2001, and references therein). Figure 4.10 indicates that there is high activity during the months of March, April, May, September and November with a peak in October. The lowest activity is during the month of June. However, it should be mentioned that these results do not imply that transformer failures in the power system can only occur during the high activity months, as intense geomagnetic storms can also occur during low activity months.

The solar cycle variation was investigated only for Hermanus because of data limitations for the years 1993-1995 which were included in order to extend the

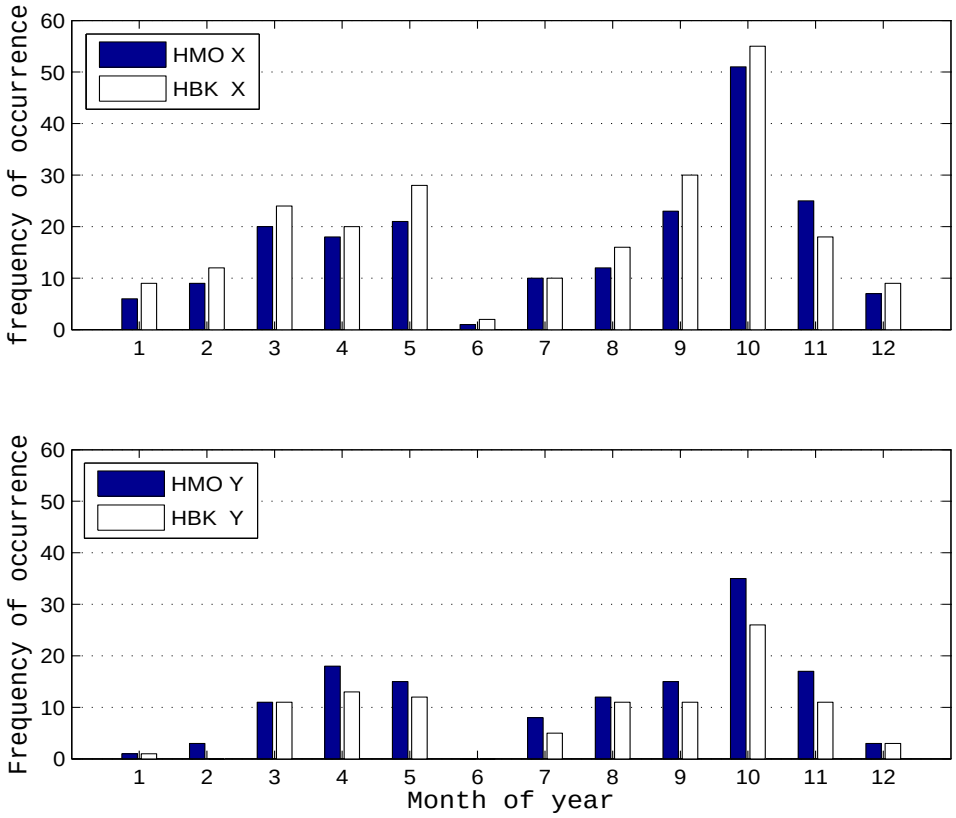

Figure 4.10: Comparison of the seasonal variation at Hermanus (HMO) and Hartebeesthoek (HBK) for the X and Y components of the HSD. Only HSD values greater than 15 nT were considered.

period of study. The results of this investigation for the X component are presented in Figure 4.11. There is no significant correlation with the maximum and minimum of the solar cycle. In Figure 4.11 there are a number of higher activity periods during 1994 and 2001 which do not conform to expectations based on the solar cycle alone. Further investigation shows that this trend agrees with results by Singh *et al.* (2005) who did a similar investigation of geomagnetic storms in India. Also interesting to note is the peak in activity during the year 2003 which includes the well known 'Halloween storm' of 29-31 October, 2003 discussed in many papers (e.g. Beamish *et al.*, 2002; Kappenman, 2005; Thomson *et al.*, 2005, and references therein).

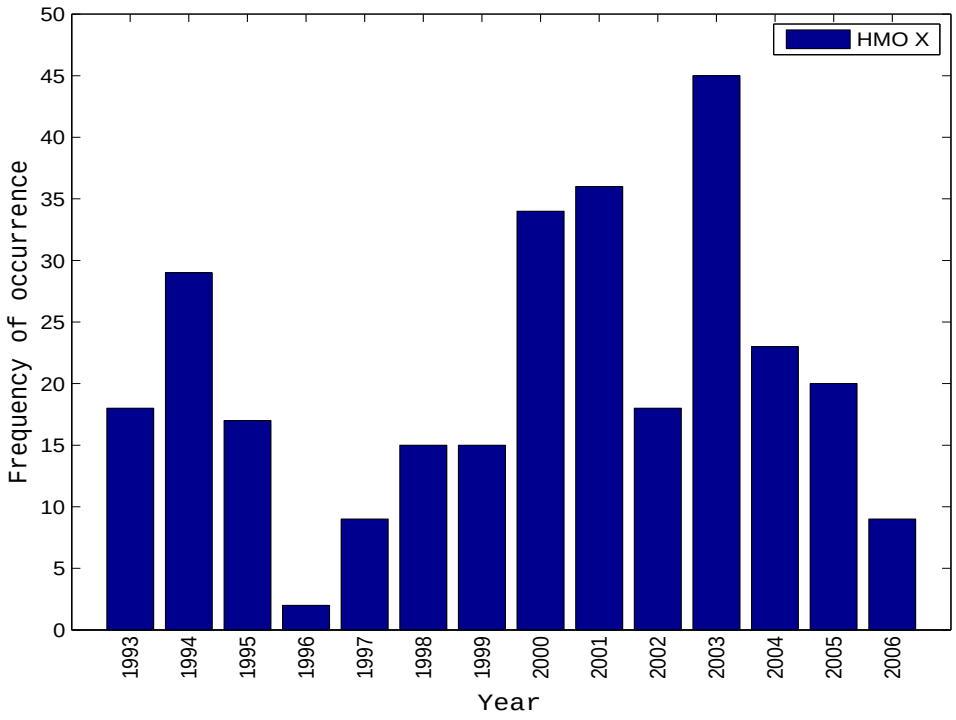

Figure 4.11: Solar cycle variation from the HSD for the years 1993-2006 at Hermanus.

4.6 Correlations of HRI and HSD with measured GIC data

The analyses in the previous two sections were carried out using model GIC data. Here measured GIC data is used for the period 29-31 October 2003. The results given in Table 4.3 show that there is an improvement in the correlation coefficients when measured data is used as compared to the model data for the same period. However, these results are not conclusive as the sample space is very small and are meant only to illustrate the need for measured GIC data.

The CCs for Max-Max in the X and Y are still very low. The correlation of the GIC with the geomagnetic field rate of change is different for Hermanus and Hartebeesthoek. Hartebeesthoek has higher CCs for dX/dt than Hermanus, but Hermanus has higher CCs for dY/dt. The difference in the correlation is linked to

Table 4.3: Summary of correlation coefficients of HRI and HSD for Hermanus (HMO) and Hartebeesthoek (HBK) using measured GIC data for the 29-31 Oct. 2003 events with 72 data points.

GIC	Geomagnetic index	X		Y	
		HMO	HBK	HMO	HBK
Max	Max	0.0677	-0.0406	0.3904	0.3449
Max	HSD	0.8250	0.8082	0.8463	0.7979
Max	HRI	0.8341	0.8197	0.8580	0.8451
		dX/dt		dY/dt	
		HMO	HBK	HMO	HBK
Max	Max	0.6103	0.6638	0.8952	0.8332
Max	HSD	0.6396	0.6734	0.8973	0.8588
Max	HRI	0.6120	0.6444	0.8878	0.8368

the positions of the two observatories with respect to the GIC site. The map in Figure 4.12 shows the positions of the geomagnetic stations relative to the Grassridge GIC substation. Hermanus and the GIC site are approximately on the same geomagnetic latitude with a separation distance of about 590 km, whereas Hartebeesthoek is roughly 892 km north-east of Grassridge.

Interestingly, the east-west components are better correlated to the GIC than the north-south components for both Hermanus and Hartebeesthoek. The difference in correlations for the different components clearly reflects the orientation of the power line as noted before. The GIC flowing in power lines corresponds differently to the north-south and east-west geoelectric field components in association with the respective temporal changes of the geomagnetic field components (Kataoka and Pulkkinen, 2008, and references therein). Pirjola (2002a) reports that it is sometimes claimed that east-west oriented power lines are more prone to large GICs than north-south oriented. According to a map of the network configuration by Koen (2002) the power line feeding into the Grassridge substation is roughly north-south oriented, corresponding with east-west dY/dt which gives rise to the north-south geoelectric field.

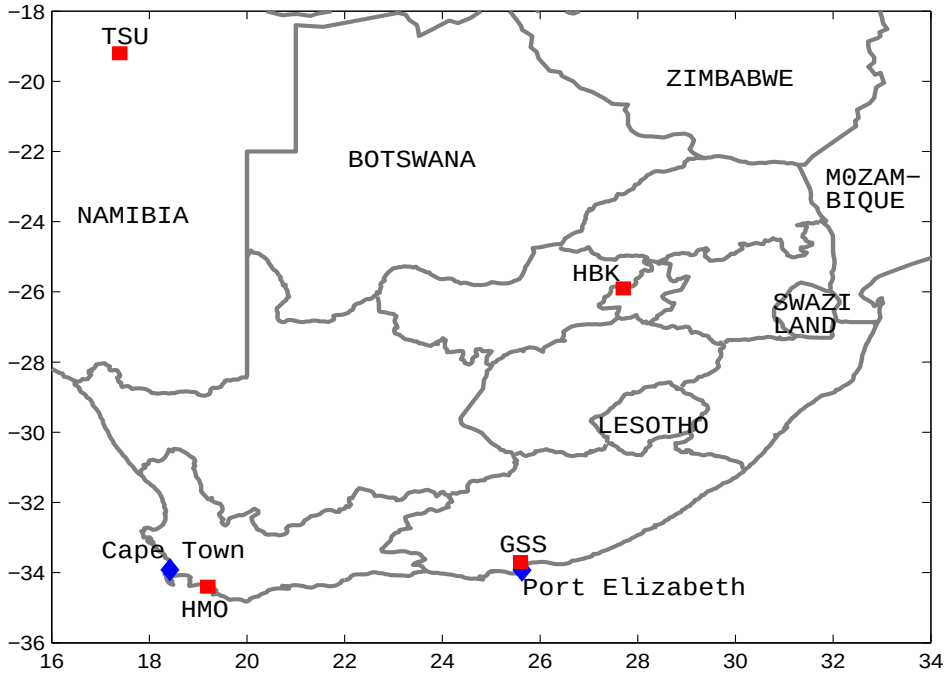

Figure 4.12: A map showing the positions (red squares) of geomagnetic observatories at Hermanus (HMO), Hartebeesthoek (HBK) and Tsumeb (TSU) and the Grassridge substation (GSS) GIC site.

4.7 Discussion

Monitoring of GICs in power systems is perhaps the most economical means of assisting power companies to reduce failures that may arise due to severe effects of space weather. In order to carry out an effective mitigation process would require not only an understanding of the geomagnetic processes which give rise to GICs, but also an understanding of the power system as a whole.

Although the K-index corresponds well with the GIC in the same interval in which a given 3-hour K-index value occurs, the index does not adequately describe the local conditions that would indicate potential GIC activity in the power grid nec-

essary for power system operators to implement mitigation procedures. Therefore, another index is needed for monitoring GICs.

Large GICs are usually associated with rapid variations in the geomagnetic field (Kappenman, 2005; Kataoka and Pulkkinen, 2008). The rate of change of the geomagnetic field has been used in many cases as a proxy for GIC (Viljanen *et al.*, 2001; Trichtchenko and Boteler, 2004; Kappenman, 2005, and references therein). Here, it was shown that for Hermanus data, the peak rate of change in the geomagnetic field correlates well with the peak GIC determined in the same interval, and agrees with results by Trichtchenko and Boteler (2004) and Kataoka and Pulkkinen (2008).

In this study it was demonstrated that the HRI of the horizontal geomagnetic field correlates well with the GIC; also that the HRI in the X-direction (north-south) has a better correlation with the peak GIC than the maximum hourly rate of change dX/dt and vice-versa for the Y components. These observations are true for a particular network configuration such as the one described for Grassridge. Both indices are used at the Regional Warning Center in Ottawa, Canada for geomagnetic forecasting.

There is a general tendency for more events to occur in the X component than in the Y component for the HSD, as also found by Beamish *et al.* (2002). Nevertheless, the fact that there are a number of events in the Y component implies that the components of the B-field in both directions must be considered when modelling the GICs in the power grid. This is so because when induction effects are considered, the geoelectric field driving the GICs in power conductors can have large values in any direction (Pirjola, 2002a). Kappenman *et al.* (1997) warn that geomagnetic storms are an ever-present risk for power grids as intense geomagnetic activity which cause large GICs can occur at any time of the day and during any time of the solar cycle. To argue this point, Kappenman *et al.* (1997) give an example of the February 1986 magnetic storm which occurred during solar minimum but almost caused a voltage collapse across the New England and mid-Atlantic regions of the USA.

Correlations between the peak GIC and all the indices show a very strong directional sensitivity which is consistent with the power line direction. GICs flow in the direction of the power line and thus the component of the geomagnetic field perpendicular to the power line is better correlated to the GIC, as discussed by Trichtchenko and Boteler (2006). Trichtchenko and Boteler (2004) found that the best fitting geomagnetic component results were different for each power system site. Here, only one GIC site was investigated, but there exists a need to extend this investigation to other sites. This, of course, is dependent on a number of factors, among which is the availability of GIC data.

The task of choosing the best index can only be done by using measured GIC data. However, it has been shown here that the hourly range index, the rate of change in the geomagnetic field and the hourly standard deviation have a good correlation with the GIC. In conclusion, it is argued that given measured GIC data, the studies carried out here are likely to yield much higher correlations.

Chapter 5

Conclusions and future work

5.1 Summary of the thesis

The thesis began by looking at the origins of space weather and solar-terrestrial conditions which cause disturbances in magnetospheric current systems. Then the geophysical aspect of GICs was discussed by investigating the ground conductivity and the methods available for modelling the geoelectric field. A new method of determining the network coefficients introduced by Pulkkinen *et al.* (2007) was used in the engineering aspect of GICs. Further, a statistical estimate of the occurrence of GICs on the power network was conducted for the Grassridge GIC site. Finally, the basic characteristics of the GIC events were studied, firstly, by determinating the behaviour pattern of the geomagnetic field and its time derivatives, and secondly, by determining and assessing the correlations between the GIC and specific local geomagnetic indices.

5.2 Conclusions

A number of aspects within the field of GICs were investigated and reported on in this thesis. The main conclusions were:

- The geoelectric field is a key parameter in the modelling of GICs. Accurate determination of the geoelectric field depends on the ground conductivity model. The ground conductivity was investigated by utilising magnetotelluric methods and a 10-layer ground conductivity model was derived for the

Grassridge GIC site in South Africa.

By using the geomagnetic field and GIC data, it was possible to modify previous values of the network coefficients used by Koen (2002) for the Grassridge GIC site. The method applied to modify the network coefficients is simple and requires a knowledge of only one network coefficient. The modified coefficients showed an improvement in ability to predict the given data.

Finally, it was shown that the layered ground conductivity model and modified network coefficients improve the modelling of GICs. A comparison of the measured GIC and the modelled GIC (computed using geomagnetic field data from Hermanus, Hartebeesthoek and Tsumeb observatories) was carried out. It was then established that the 10-layer ground conductivity model is only valid for the Hermanus Geomagnetic Observatory and Grassridge GIC site pair.

- The statistical risk analysis for the Grassridge GIC site points to the existence of $|\text{GIC}| > 5$ A, which poses a risk to power transformers on the network. This is of concern, since such currents can drive power transformers into saturation.

- The local K-index does not adequately describe the local conditions as would be required for the estimation of the expected GIC activity on the power grid.

- The characteristics of GICs were investigated by determining and assessing the correlation between the GIC index and the different local geomagnetic indices.

  The geomagnetic field rate of change, the hourly range index and the hourly standard deviation were studied and were found to correlate well with the GIC. The three indices should be considered for further investigation, using measured GIC data. It was established that the HRI of the horizontal geomagnetic components X (north-south) and Y (east-west) correlate better with the hourly peak GIC than the HSD of the horizontal geomagnetic components X and Y.

- The geomagnetic field X and Y local indices show a very strong directional sensitivity, consistent with the power line direction. The results show that there is better correlation between the peak hourly GIC and the east-west components of the local indices than the north-south components. These results are consistent with the north-south geoelectric field and the power line orientation.

  It was established that each geomagnetic observatory has a different directional preference with respect to the GIC site. Therefore, it is important to consider both the X and Y horizontal geomagnetic components and use geomagnetic observation data nearest to the GIC site.

- These studies should be extended to other GIC sites. The conclusions drawn here are particular to the Grassridge electrical substation GIC site unless stated otherwise. The Southern African power network is large and these findings cannot be extended to other sites before actual studies are done.

Lastly, it is important to stress that GIC studies within mid-latitude Southern African region are hampered by the lack of measured GIC data. At the time of writing this thesis only two GIC monitoring sites were known. The situation is aggravated by the small number of magnetic observatories covering this vast region. This makes it challenging to model and determine the impact of GICs on the network. However, transformer failures experienced at substations on the South African and Namibia networks suggest that there exists a strong necessity to improve the modelling efficiency.

5.3 Challenges for future work

Many questions and developments to be explored in future GIC studies arise from this work. Some of these are:

- A new set of network coefficients has been introduced. However, the network coefficient b differs significantly from the value obtained by Koen (2002). There is a need to further investigate properties of the network coefficients.

- The derived layered conductivity model is only valid for the specific geomagnetic observatory and GIC site. All these investigations were centred on the Grassridge GIC site. It is important that a representative conductivity model be developed for the whole of South Africa in order to predict currents flowing in the entire power grid. These studies should be extended to other regional power networks.

- The statistical risk analysis for the Grassridge GIC site shows that the level of currents induced on the power network is very low compared to what has been experienced in other networks, for example in Finland. Considering the level of currents observed, it is necessary that the main cause of transformer failures are investigated. Transformer failures experienced in the past can be linked either to the transformer types or to the power system design. To effectively execute this task will require collaboration with the power companies concerned.

- The geomagnetic range indices, the hourly standard deviation and the geomagnetic field rate of change will have to be further investigated using measured GIC data. The major task that lies ahead is to determine index thresholds for each GIC site that can be used for monitoring the GICs.

- A strong geomagnetic field directional sensitivity was observed with respect to the Grassridge site. The true directional preference is a matter that should be investigated using approaches similar to those of Boteler *et al.* (1994), Viljanen *et al.* (2001) and Trichtchenko and Boteler (2004).

In conclusion, this thesis presents a first look into the requirements for characterising GICs, which will eventually lead to a prediction tool for GIC events, a tool that will prove extremely useful to Southern African power companies.

References

Amm O. "Ionospheric elementary current systems in spherical coordinates and their application". J. Geomag. Geoelectr., vol. 49, pp. 947–955, 1997.

Amm O. and Viljanen A. "Ionospheric disturbance magnetic field continuation from the ground to the ionosphere using spherical elementary current systems". Earth Planet. Space, vol. 51, pp. 431–440, 1999.

Beamish D., Clark T.G.D., Clarke E. and Thomson A.W.P. "Geomagnetically induced currents in the UK: Geomagnetic variations and surface electric fields." J. Atmos. Sol. Terr. Phys., vol. 64, pp. 1779–1792, 2002.

Bernhardi E. *Modelling geomagnetically induced currents in Southern Africa*. BSc. Honours Project, University of Cape Town, 2006.

Boerner W.M., Cole J.B., Goddard W.R., Tarnawecky M.Z., Shafai L. and Hall D.H. "Impact of solar and auroral storms on power line systems". Space Sci. Rev., vol. 35(2), pp. 195–205, 1983.

Boteler D.H. "Space weather effects on power systems". in Song D., Singer H.J and Siscoe G.L. *Space Weather*. American Geophysical Union, pp. 347–352, 2001.

Boteler D.H., Bui-Van Q. and Lemay J. "Directional sensitivity of geomagnetically induced currents of the Hydro-Quebec 735 kV power system". IEEE Trans. Power Delivery, vol. 9(4), pp. 1963–1971, 1994.

Campbell W.H. *Introduction to geomagnetic fields*. Cambridge University Press, 1997.

Chave A.D. and Thomson D. "Bounded influence magnetotelluric response function estimation". Geophys. J. Int., vol. 157, pp. 988–1006, 2004.

Constable S.C. "Resistivity studies over the Flinders conductivity anomaly, South Australia". Geophys. J. R. Astr. Soc., vol. 83, pp. 775–786, 1985.

Gaunt C.T. and Coetzee G. "Transformer failure in regions incorrectly considered to have low GIC-risks". IEEE Power Tech., Conference Paper 445, Lausanne, July, 2007.

Hamilton M.P., Jones A.G., Evans R.L., Evans S., Fourie C.J.S., Garcia X., Mountford A. and Spratt J.E. "Electrical anisotropy of South Africa lithosphere compared with seismic anisotropy from shear-wave splitting analyses". Phys. Earth Planet. Interiors, vol. 158, pp. 226–239, 2006.

Hjärten M. *Master thesis in interpretation of controlled-source radiomagnetotelluric data from Hallandsåsen.* Master's thesis, Uppsala University, 2007.

Huttunen K.E.J., Koskinen H.E.J., Pulkkinen T.I., Pulkkinen A., Palmroth M., Reeves E.G.D. and Singer H.J. "April 2000 magnetic storm: Solar wind driver and magnetospheric response". J. Geophys. Res., vol. 107(A12), pp. 1440, doi:10.1029/2001JA009154, 2002.

Jordanova V.K., Thorne R.M., Farrugia C.J., Dotan Y., Fennell J.F., Thomson M.F., Reeves G.D. and McComas D.J. "Ring current dynamics during the 13-18 July 2000 storm period". Sol. Phys., vol. 204, pp. 361–375, 2001.

Joselyn J.A. "Geomagnetic activity forecasting: The state of the art". Rev. Geophys., vol. 33(3), pp. 383–401, 1995.

Kappenman J.G. "An overview of the impulsive geomagnetic field disturbance and the power grid impacts associated with the violent Sun-Earth connection events of 29-30 October 2003 and a comparative evaluation with other contemporary storms". Space Weather, vol. 3, S08C01, doi:10.1029/2004SW000128, 2005.

Kappenman J.G., Radasky W.A., Gilbert J.L. and Erinmez I.A. "Advanced geomagnetic storm forecasting: A risk management tool for electric power system operations". IEEE T. Plasma Sci., vol. 28, pp. 2114–2121, 2000.

Kappenman J.G., Zanetti L.J. and Radasky W.A. "Geomagnetic storms can threaten electric power grid". Earth in Space, vol. 9(7), pp. 9–11, 1997.

Kataoka A. and Pulkkinen A. "Geomagnetically induced currents during intense storms driven by coronal mass ejections and corotating interacting regions". J. Geophys. Res., vol. 113, A03512, doi:10.1029/2007JA012487, 2008.

Kivelson M.G. and Russell C.T. *Introduction to space physics.* Cambridge University Press, 1995.

Koen J. *Geomagnetically induced currents in the Southern African electricity transmission network.* Ph.D. thesis, University of Cape Town, 2002.

Lehtinen M. and Pirjola R. "Currents produced in earthed conductor by geomagnetically induced electric fields". Ann. Geophys., vol. 3(4), pp. 479–484, 1985.

Matsushita S. and Campbell W.H. *Physics of geomagnetic phenomena.* Academic Press, 1967.

McKay A.J. *Geoelectric fields and geomagnetically induced currents in the United Kingdom.* Ph.D. thesis, University of Edinburgh, 2003.

Menvielle M., Papitashvili N., Häkkinen L. and Sucksdorff C. "Computer production of the K indices: review and comparison of methods". Geophys. J. Int., vol. 123(3), pp. 866–886, 1995.

Molinski T.S. "Why utilities respect geomagnetically induced currents". J. Atmos. Sol. Terr. Phys., vol. 64, pp. 1765–1778, 2002.

Nishida A. *Geomagnetic diagnosis of the magnetosphere.* Springer-verlag, 1978.

Pellerin L., Johnston J.M. and Hohmann G.W. "A numerical evaluation of electromagnetic methods in geothermal exploration". Geophysics, vol. 61(1), pp. 121–130, 1996.

Pirjola R. "Induction in power transmission lines during geomagnetic disturbances". Space Sci. Rev., vol. 35(1), pp. 185–193, 1983.

Pirjola R. "Geomagnetically induced currents during magnetic storms". IEEE Trans. Plasma Sci., vol. 28(6), pp. 1867–1873, 2000.

Pirjola R. “Fundamentals about the flow of geomagnetically induced currents in a power system applicable to estimating space weather risks and designing remedies”. J. Atmos. Sol. Terr. Phys., vol. 64, pp. 1967–1972, 2002a.

Pirjola R. “Geomagnetic effects on ground-based technological systems”. Rev. Radio Sci. (URSI), pp. 473–496, 2002b.

Pirjola R. “Review on the calculation of the surface electric and magnetic fields and geomagnetically induced currents in ground based technological systems”. Surv. Geophys., vol. 23, pp. 71–90, 2002c.

Pirjola R. and Boteler D.H. “Calculation methods of the electric and magnetic fields at the Earth’s surface produced by a line current”. Radio Sci., vol. 37(3), 1042, doi:10.1029/2001RS002576, 2002.

Pulkkinen A. *Geomagnetic induction during highly disturbed space weather conditions: Study of ground effects.* Ph.D. thesis, University of Helsinki, 2003.

Pulkkinen A., Pirjola R. and Viljanen A. “Determination of the ground conductivity and system parameters for optimal modeling of geomagnetically induced current flow in technological systems”. Earth Planet. Space, vol. 59, pp. 999–1006, 2007.

Richardson I.G., Cliver E.W. and Cane H.V. “Sources of geomagnetic storms for solar minimum and maximum conditions during 1972-2000”. Geophy. Res. lett., vol. 28(13), pp. 2569–2572, 2001.

Rosenqvist L., Opgenoorth H., Buchert S., McCrea I., Amm O. and Lathuillere C. “Extreme solar-terrestrial events of October 2003: High-latitude and cluster observations of the large geomagnetic disturbances on 30 October”. J. Geophys. Res., vol. 110, A09S23, doi:10.1029/2004JA01927, 2005.

Simpson F. and Bahr K. *Practical magnetotellurics.* Cambridge University Press, 2005.

Singh B., Dubey S.C., Tiwari D.P. and Tripathi A.K. “The study of large geomagnetic storms observed during period 1986-2002”. 29th International Cosmic Ray Conference, Pune, vol 2, pp. 299–302. 2005.

Thomson A.W.P., Clarke E., McKay A. and Reay S.J. "Surface electric fields and geomagnetically induced currents in Scottish Power grid during 30 October 2003 geomagnetic storm". Space Weather, vol. 3, S11002, doi:10.1029/2005SW00156, 2005.

Trichtchenko L. and Boteler D.H. "Modeling geomagnetically induced currents using geomagnetic indices and data". IEEE Trans. Plasma Sci., vol. 32(4), pp. 1459–1469, 2004.

Trichtchenko L. and Boteler D.H. "Response of the power systems to the temporal characteristics of geomagnetic storms". Electrical and Computer Engineering, CCECE'06. Canadian Conference on Electrical and Computer Engineering, IEEE, Ottawa, pp. 390–393. 2006.

Viljanen A. "The relation between geomagnetic variations and their time derivatives and implications for estimation of induction risks". Geophys. Res. Lett., vol. 24(6), pp. 631–634, 1997.

Viljanen A., Nebanlinna H., Pajunpää K. and Pulkkinen A. "Time derivative of the horizontal geomagnetic field as an activity indicator". Ann. Geophys., vol. 19, pp. 1107–1118, 2001.

Viljanen A. and Pirjola R. "Statistics on geomagnetically induced currents in the Finnish 400 kV system based on the recordings of geomagnetic variations". J. Geomag. Geoelectr., vol. 41, pp. 411–420, 1989.

Viljanen A. and Pirjola R. "Geomagnetically induced currents in the Finnish high-voltage power system". Surv. Geophys., vol. 15, pp. 383–408, 1994.

Viljanen A., Pulkkinen A., Amm O., Pirjola R., Korja T. and BEAR Working Group. "Fast computation of the geoelectric field using the method of elementary current systems and planar Earth model". Ann. Geophys., vol. 22(1), pp. 101–113, 2004.

Viljanen A., Pulkkinen A., Pirjola R., Pajunpää K., Posio P. and Kiostinen A. "Recordings of geomagnetically induced currents and a nowcasting service of the Finnish natural gas pipeline". Space Weather, vol. 4, S10004, 2006.

Walker A.D.M. *Magnetohydrodynamic waves in geospace*. IOP Publishing, 2005.

Weckmann U., Ritter O., Jung A., Branch T. and Wit M.D. "Magnetotelluric measurements across the Beattie magnetic anomaly and the Southern Cape conductive belt, South Africa". J. Geophys. Res., vol. 112, B05416, doi:10.1029/2005JB003975, 2007.

Zatjirua T. *Investigation of geomagnetically induced currents in the transmission network of Namibia*. BSc. Engineering Project, University of Cape Town, 2005.

Zhang J., Liemohn M.W., Kozyra J.U., Lynch B.J. and Zurbuchen T.H. "A statistical study of the geoeffectiveness of magnetic clouds during high solar activity years". J. Geophys. Res., vol. 109, A09101, doi:10.1029/2004JA010410, 2004.